Properties of hyperons in nuclear matter from chiral hyperon-nucleon interactions at next-to-next-to-leading order

Asanosuke Jinno [*]
Department of Physics, Faculty of Science, Kyoto University, Kyoto 606-8502, Japan

Johann Haidenbauer [†]
Institute for Advanced Simulation (IAS-4), Forschungszentrum Jülich, D-52425 Jülich, Germany

Ulf-G. Meißner [‡]
Helmholtz-Institut für Strahlen- und Kernphysik and Bethe Center for Theoretical Physics, Universität Bonn, D-53115 Bonn, Germany;
Institute for Advanced Simulation (IAS-4), Forschungszentrum Jülich, D-52425 Jülich, Germany;
and Peng Huanwu Collaborative Center for Research and Education,
International Institute for Interdisciplinary and Frontiers, Beihang University, Beijing 100191, China

(Received 4 October 2025; accepted 17 November 2025; published 22 December 2025)

The Λ and Σ single-particle potentials in infinite nuclear matter are analyzed within a recently established chiral hyperon-nucleon (YN) interaction up to N^{2}LO in combination with a nucleon-nucleon interaction derived in the same scheme. The self-consistent Brueckner-Hartree-Fock method with the continuous choice of the single-particle potential is employed. It is found that the Λ single-particle potential is comparable to the results achieved with the NLO YN interaction from 2019. The resulting Σ potential becomes more attractive compared to the previous NLO results due to the constraint from the recent ΣN differential cross section data measured in the J-PARC E40 experiment. An estimate of the theoretical uncertainty of the single-particle potentials is provided in terms of the truncation error in the chiral expansion.

DOI: 10.1103/vs4h-p3zh

I. INTRODUCTION

Due to the limited amount of direct experimental information on the interaction of the hyperons Λ and Σ with nucleons, see Ref. [1] for a recent overview, it is essential to consider also their interaction in few- and many-body systems as a test and as an additional source of information. This aim can be achieved within so-called *ab initio* calculations where the elementary hyperon-nucleon (YN) interaction is used as input in Faddeev-Yakubovsky equations [2–5] or in the no-core shell model [6–10] in order to evaluate the properties of light Λ hypernuclei. A similar strategy is also followed in studies within nuclear lattice effective field theory [11]. For heavier hypernuclei traditionally microscopic calculations have been performed with an effective YN interaction, which is generated from the G matrix, i.e., from the solution of the Bethe-Goldstone equation in infinite nuclear matter for the underlying bare YN potential [12–17].

The YN G matrix is also a key element in microscopic studies of compact objects like neutron stars [18–21] in the context of the so-called "hyperon puzzle;" see, e.g., Refs. [22–30] and recent reviews [31–34]. Here, "puzzle" refers to the quest to reconcile the seemingly contradictory observations that in calculations with standard YN interactions Λ's (and possibly other hyperons) appear with increasing density, thereby causing a softening of the equation of state (EOS), while the observed mass-radius relation and the maximum mass of neutron stars can be explained only with a stiff EOS. Clearly, while for the application in finite nuclear matter the G matrix is usually used around nuclear matter saturation density, $\rho_0 = 0.16$ fm^{-3}, or below, with regard to neutron stars the relevant region extends very well up to (6–7)ρ_0.

For many years phenomenological YN potentials have been used as a starting point for such microscopic calculations. However, this has changed in recent years with the arrival of YN potentials derived within chiral effective field theory (EFT). That approach with an inherent power counting, initially suggested by Weinberg for application to the nucleon-nucleon (NN) interaction, allows one to improve the results order by order and, equally importantly, enables also an estimation of the theoretical uncertainty. This is not only valid for the elementary YN interaction but applies also for few- and many-body studies where chiral YN interactions are employed.

In the present work we investigate the in-medium properties of the Λ and Σ hyperons employing chiral YN interactions. The study is performed within the conventional Brueckner theory [35–37] at first order in the hole-line expansion, i.e., the so-called Brueckner-Hartree-Fock (BHF)

[*]Contact author: jinno.asanosuke.36w@st.kyoto-u.ac.jp
[†]Contact author: j.haidenbauer@fz-juelich.de
[‡]Contact author: meissner@hiskp.uni-bonn.de

approximation. The starting point is the new YN potential published recently by the Jülich-Bonn group [1], based on SU(3) chiral effective field theory up to next-to-next-to-leading order (N^2LO). Besides extending the chiral order with respect to our earlier next-to-leading order (NLO) YN potentials from 2013 (NLO13) [38] and 2019 (NLO19) [39], the new YN interaction builds also on a novel regularization scheme, the so-called semilocal momentum space regularization, which has been shown to work rather well in the nucleon-nucleon (NN) sector [40]. Furthermore, the potential incorporates new constraints from $\Sigma^- p$ and $\Sigma^+ p$ differential cross sections measured in the J-PARC E40 experiment [41–43]. The new semilocal momentum space regularized (SMS) interactions are also the first YN potentials where the separation energies of light Λ hypernuclei can be rather well described [44].

Our study has two goals. One of them is to provide a general overview of the in-medium properties that result from the new SMS YN potentials. The other one, and maybe the more important one, is to explore the convergence pattern of the chiral expansion and the regulator dependence of the properties of hyperons in nuclear matter. Specifically, we provide a first uncertainty estimate for the Λ and Σ single-particle potentials, following corresponding efforts for nucleons in infinite nuclear matter [45,46]. So far in nuclear matter calculations with chiral YN potentials only the cutoff dependence has been used to estimate the uncertainty [47–50].

An additional aspect we want to address is the influence of YN P waves on the matter properties. Since experimental information on Λp differential cross sections at low momenta is rather limited [51,52], the YN interaction in the P waves cannot be determined reliably. In the case of NLO13 (NLO19) [38,39] the smallness of the Λp cross section above the ΣN threshold, i.e., at around $p_{\rm lab} \approx 800$ MeV/c, was used as a guideline to fix the strength of the P-wave interactions, together with constraints from the corresponding NN P-wave interactions provided by the underlying SU(3) flavor symmetry. Agreement with the Λp data could be only achieved if the individual contributions from all the P waves ($^1P_1$, $^3P_0$, $^3P_1$, $^3P_2$) are kept small, which means in turn that the corresponding phase shifts have to be small. As already mentioned, in the SMS YN potential $\Sigma^- p$ and $\Sigma^+ p$ differential cross sections, measured at J-PARC [41–43], have been used to constrain the P waves. However, also in this case a unique determination of all P-wave interactions was not possible [1].

We restrict our study to densities up to twice the nuclear matter saturation density $\rho_0 = 0.16$ fm^{-3}, i.e., to Fermi momenta below $k_F = 2.15$ fm^{-1} ($\approx$400 MeV) in pure neutron matter (PNM). This limit on the density is suggested by the breakdown scale of the chiral expansion [53,54] and by the cutoff values applied in the regulators of the chiral potentials [1,38,39], which are both in the order of 500 ± 100 MeV. See also the corresponding comments in Refs. [45,55]. Moreover, since the presence of the Pauli operator in the G-matrix equation suppresses the contributions from lower momenta in nuclear matter calculations one is automatically more sensitive to the high-momentum part and that means to regulator artifacts. Extrapolations to higher density are, of course, always possible, but one should keep in mind that they are predominantly of phenomenological nature.

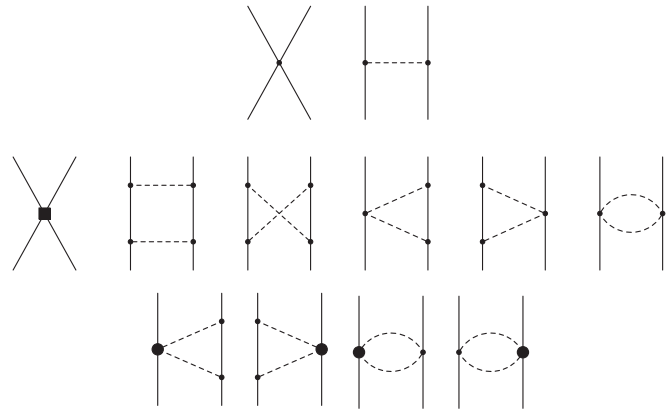

FIG. 1. Diagrams contributing to the YN potential at LO (top), NLO (center), and N^2LO (bottom) in chiral EFT. Solid and dashed lines denote octet baryons and pseudoscalar mesons, respectively.

The paper is structured in the following way. Section II briefly introduces the baryon-baryon interactions employed in this work and then the Brueckner theory. In Sec. III we provide results for the single-particle potentials of the Λ and the Σ in symmetric nuclear matter (SNM) and in PNM. We focus on the results at nuclear matter saturation density, but we also discuss the density and the momentum dependence of the single-particle potentials. In Sec. IV we perform an estimate of the theoretical uncertainty of our results for the hyperon single-particle potentials due to the truncation in the chiral expansion, the first of its kind. The paper ends with a brief summary and an outlook.

II. THEORETICAL COMPONENTS

A. Hyperon-nucleon and nucleon-nucleon interactions

Recently the Jülich-Bonn group has established a YN potential for the strangeness $S = -1$ sector (ΛN, ΣN) up to N^2LO in the chiral expansion [1]. The main focus of the present work is to explore the in-medium properties of Λ and Σ that follow from this interaction. Below we briefly summarize the main features and merits of this interaction. For a detailed description we refer the reader to the original publication.

The YN interaction is derived within SU(3) chiral effective field theory with the Weinberg power counting applied to the potential. At LO one-meson exchange diagrams and nonderivative four-baryon contact terms contribute to the potential; see Fig. 1 (top). At NLO additional contact terms and (irreducible) two-meson exchange diagrams at the one-loop level contribute (center). Finally, at N^2LO two-meson exchange contributions involving the subleading meson-baryon Lagrangian arise (bottom). The contributions from pseudoscalar-meson exchanges (π, η, K) are, in principle, fixed by the assumed SU(3) flavor symmetry. The symmetry provides relations between the coupling constants at the various meson-baryon-baryon vertices so that they all can be written in terms of the F and D couplings of the underlying

meson-baryon interaction Lagrangian [38,56]. F and D satisfy the relation $F + D = g_A \approx 1.27$, where g_A is the axial-vector strength measured in neutron β decay. In contrast the contact terms represent the unresolved short-distance dynamics and the associated low-energy constants (LECs) are essentially free parameters. In practice, they are fitted to low-energy YN scattering data and additionally constrained by the hypertriton ($^3_\Lambda$H) binding energy. At the order considered the contact terms yield contributions to the S and P waves of the potential.

Although SU(3) flavor symmetry is imposed for constructing the interaction, the explicit SU(3) symmetry breaking by the physical masses of the pseudoscalar mesons (π, K, η) is taken into account when evaluating the potential. The mass differences induce also a possible SU(3) breaking in the leading-order contact terms [38,57], which is likewise considered in the YN potential of Ref. [1].

When solving the scattering equations for chiral potentials a regulator has to be introduced in order to remove high-momentum components [58]. For that, in Ref. [1] a novel regularization scheme, the so-called semilocal momentum space regularization, has been employed which has been already successfully applied in studies of the NN interaction within chiral effective field theory up to high orders [40]. The name refers to the fact that a local regulator is applied to the meson-exchange contributions, whereas the contact terms, being nonlocal by themselves, are regularized with a nonlocal function. The cutoff masses entering the regulator function considered in Ref. [1] are in the range of 500–600 MeV. For comparison, the cutoffs employed in the SMS NN interaction are in the range 350–550 MeV [40].

With the NLO and N^{2}LO SMS YN potentials an excellent description of the low-energy Λp, $\Sigma^- p$, and $\Sigma^+ p$ scattering cross sections could be achieved, resulting in a total χ^2 of 15–16 for the commonly considered 36 data points [38]. Clearly, those data are primarily sensitive to the YN interaction in the S waves and, accordingly, only the LECs contributing to the S-wave potential could be reliably fixed. Nonetheless, in addition, new measurements of angular distributions for the ΣN channels from J-PARC [41–43] have been analyzed in an attempt to determine also the strength of the contact interactions in the P waves.

It is also noteworthy to mention that the SMS YN potentials have been utilized in calculations of light Λ-hypernuclei, based on the Faddeev-Yakubovsky approach and the no-core shell model (so far up to $A \approx 8$). The results, reported in Refs. [44,59], show that the separation energies based on the two-body interaction alone are already fairly close to the experimental values [60]. When chiral (ΛNN, ΣNN) three-body forces are included, which arise at N^{2}LO in the chiral expansion [61], a quantitative agreement with the experimental separation energies is achieved.

Besides the SMS YN potentials we will also present results for the earlier NLO YN potentials developed by the Jülich-Bonn-Munich and Jülich-Bonn groups, NLO13 [38] and NLO19 [39], that are based on a different regularization scheme. In those potentials a nonlocal regulator is used for all components, with a cutoff mass ranging from 500 to 650 MeV. We include here the results based on the NLO13 and NLO19 potentials with 500 MeV. Those are the potentials employed in the study of the hyperon puzzle by Gerstung *et al.* [19]. Indeed, among the NLO13 and NLO19 YN potentials those with cutoff 500 MeV yield each the most attractive results for U_Λ at ρ_0. We note that the results of those potentials for the Λp and ΣN cross sections at low energies are practically identical to the ones by the SMS YN interaction [1,38,39].

Regarding the NN interaction we employ the corresponding SMS potentials by Reinert *et al.* [40] for consistency reasons. Specifically, we use the potentials with the highest order in the chiral expansion, namely N^{4}LO$^+$ in the notation of Ref. [40].

B. Brueckner theory

We utilize conventional Brueckner theory to calculate the single-particle potential of hyperons in nuclear matter using the YN interactions in free space. Here, we briefly summarize the basics of the formalism and provide the essential formulas. A detailed description can be found in Ref. [48]; see also Refs. [62–66].

Within the Brueckner theory, the two-body potential V in free space is converted into an effective two-body interaction in medium, the G matrix, which is evaluated by solving the Bethe-Goldstone equation

$$G(\omega) = V + V \frac{Q}{\omega - H_0 + i\epsilon} G(\omega), \tag{1}$$

with the so-called starting energy ω. The Pauli operator Q eliminates intermediate two-body states below the Fermi sea. The energy denominator in Eq. (1) is the difference between the starting energy ω and the total energy of the intermediate state, which includes the baryon single-particle potentials

$$\omega = E_{B_1}(k_1) + E_{B_2}(k_2),$$
$$E_{B_i}(k_i) = m_{B_i} + \frac{k_i^2}{2m_{B_i}} + \mathrm{Re}U_{B_i}(k_i). \tag{2}$$

Here, the starting energy ω is usually chosen "on-shell," i.e., it is set equal to the energy of the two particles in the initial state. The angle average of the Pauli operator and the energy denominator is adopted, so that after a standard partial-wave decomposition there remains only a one-dimensional integral equation. Nonetheless, for the hyperons Λ and Σ the channel coupling ΛN-ΣN has to be taken into account. Thus, depending on whether the G matrix is calculated in the isospin or particle basis, coupled-channel equations analogous to Eq. (1) for two or three channels have to be solved. The single-particle potential of a baryon $B_1 = (p, n, \Lambda, \Sigma^{0,\pm})$ is typically chosen as the Hartree-Fock type one:

$$U_N(k) = \sum_{m \in \text{Fermi sea}} \langle Nm|G|Nm\rangle - \langle Nm|G|mN\rangle, \tag{3}$$

$$U_Y(k) = \sum_{m \in \text{Fermi sea}} \langle Ym|G|Ym\rangle. \tag{4}$$

Note that the Bethe-Goldstone equation (1) and the single-particle potentials U_{B_i} must be evaluated self-consistently because the single-particle potential appears in Eq. (1) through the energy denominator.

The definition of the U_{B_i} in Eqs. (3) and (4) applies only to occupied states within the Fermi sea. The single-particle potential above the Fermi sea can be chosen arbitrarily and should be chosen to achieve faster convergence in the hole-line expansion. There are commonly two choices of U_{B_i}: the gap choice which omits U above the Fermi sea and the continuous choice which uses U as defined in Eqs. (3) and (4) also above the Fermi sea. There are calculations that include higher-order contributions in the hole-line expansion [67–69] and those observe a faster convergence by the continuous choice over the gap choice. The exploratory calculation of the in-medium properties of the SMS YN potentials in Ref. [1] was based on the gap choice.

In the actual calculations partial waves up to a total angular momentum of $J = 5$ are taken into account. Note that due to the local regulator used for the meson-exchange contribution the potential drops off more slowly for large momenta, which requires appropriate mesh points with large maximum momentum for calculating the G matrix.

In Ref. [55] some sort of oscillatory behavior of U_N was found in calculations with the N^{3}LO NN potential by Epelbaum *et al.* from 2005 [58] and a density-dependent NN force [70]. A similar behavior was also observed by Gerstung *et al.* [71] for the N^{3}LO NN potential by Entem and Machleidt [72]. In both calculations an additional cutoff regularization has been introduced and applied to the single-particle potential in the G-matrix equation to obtain numerically stable results. We do not observe such artificial oscillations for the SMS NN potentials up to $\rho = 2\rho_0$ and, therefore, no additional cutoff is required. In fact, also for the semilocal coordinate-space regularized (SCS) NN potentials employed in the studies of Hu *et al.* [45,46] no cutoff artifacts were found [73].

III. RESULTS

In this section we show and discuss results for the hyperon single-particle potentials. In particular, we document the momentum and density dependence of the Λ and Σ single-particle potentials predicted by the SMS YN interactions. We start with some results for nuclear matter based on the SMS NN potentials [40]. Specifically we show the predicted nucleon single-particle potential U_N. As one can see from Eq. (2), this quantity enters as input in the calculation of the in-medium properties of the hyperons.

A. Nuclear matter

Since to the best of our knowledge nuclear matter results for the SMS NN potentials of Reinert *et al.* [40] have so far not been reported, we present such results in this subsection. We focus on the potentials of highest order in the chiral expansion, namely N^{4}LO$^+$, which we use for our calculation of the hyperon properties. For comparison we present also results for the N^{3}LO potentials by Entem and Machleidt (EM) [72], which have been used by Gerstung *et al.* [19]. It should be said that the actual calculations in that reference include also an additional effective density-dependent NN interaction, derived from N^{2}LO NNN forces following the prescription of Holt *et al.* [74,75].

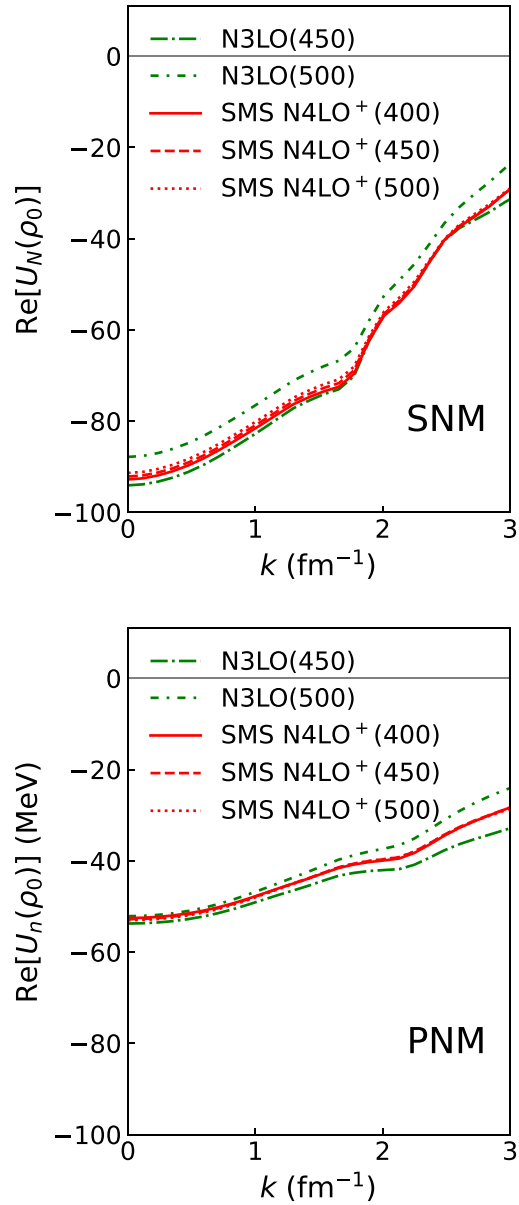

FIG. 2. Nucleon single-particle potentials in symmetric nuclear matter (top) and pure neutron matter (bottom) at ρ_0. N^{3}LO(450) and N^{3}LO(500) refer to the N^{3}LO NN potential by Entem and Machleidt [72] with corresponding cutoff, while the SMS N^{4}LO$^+$ potential is by Reinert *et al.* [40].

Nucleon single-particle potentials in SNM and in PNM at nuclear matter saturation density are shown in Fig. 2, for the EM potentials [72] with cutoffs 450 and 500 MeV and for the SMS N^{4}LO$^+$ potentials with cutoffs 400–500 MeV [40]. Remarkably the momentum dependence of U_N resulting from the SMS NN potentials exhibits basically no variation with the cutoff, testifying that the residual regulator dependence at that order of the chiral expansion is indeed very small. In the case of the EM N^{3}LO potential the cutoff variation leads to

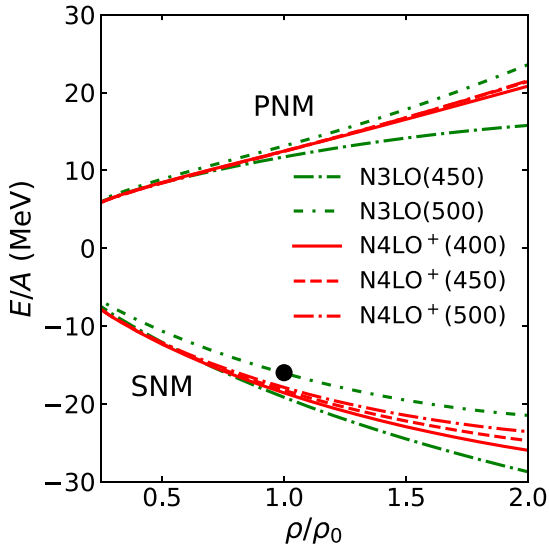

FIG. 3. Total energy per particle in both symmetric nuclear matter and pure neutron matter. Results are shown for the N^{3}LO [72] and SMS N^{4}LO$^+$ [40] *NN* potentials. The empirical value at the nuclear matter saturation point, $E/A = -16$ MeV, is indicated by a circle.

some spread in the value of U_N; however, also here the actual momentum dependence is very similar.

In the BHF approximation the total energy is given by

$$E = \sum_{m\in\text{Fermi sea}} \left[\langle m|T|m\rangle + \frac{1}{2} U_N(k_m) \right], \tag{5}$$

where T is the kinetic energy operator. In Fig. 3 results for the total energy per particle in both SNM and in PNM are shown up to $2\rho_0$, corresponding to the Fermi momentum $k_F \leqslant 1.70$ fm^{-1} for SNM and $k_F \leqslant 2.15$ fm^{-1} for PNM. The Fermi momentum is related to the density via $\rho = 2k_F^3/(3\pi^2)$ for SNM and $\rho = k_F^3/(3\pi^2)$ for PNM, respectively. Both the EM N^{3}LO and the SMS N^{4}LO$^+$ *NN* potentials yield similar results, expectedly because the underlying single-particle potentials are also very similar. The SNM results for N^{4}LO$^+$ are slightly too attractive and lie below the empirical value at the saturation point. In the case of the EM potentials there is a larger variation with the cutoff.

B. Λ in symmetric nuclear matter

We now proceed to the in-medium properties of the hyperons. The inputted U_N is calculated using the SMS N^{4}LO$^+$ *NN* force with the 450 MeV cutoff. First, we focus on the Λ single-particle potential at nuclear matter saturation density and for zero momentum, which can be compared with quasiempirical values inferred from hypernuclear experiments. Table I summarizes the results for $U_\Lambda(k=0)$ and its partial-wave decomposition. We adopt the notation from Ref. [1] and specify the various potentials by their chiral order and by the employed cutoff mass. The values of $U_\Lambda(k=0)$ predicted by the SMS N^{2}LO potentials range from −46 to −41 MeV; those of the NLO potentials are between −39 and −34 MeV. In comparison, the result for NLO19 (−41 MeV) is right in the middle of the SMS results, while the one for NLO13 (−33 MeV) is at the upper edge. Also phenomenological *YN* models predict results for U_Λ in that range [62,63,76]. The usually cited quasiempirical value, i.e., the well depths of a Λ-nucleus Woods-Saxon potential fixed in an analysis of hypernuclear data, amounts to $U_\Lambda \approx -30$ MeV [77]. A recent phenomenological analysis [78] based on hypernuclei estimates that the *YN* two-body contribution to $U_\Lambda(k=0)$ is -38.6 ± 0.8 MeV and attributes a contribution of 11.3 ± 1.4 MeV to repulsive three-body forces.

It is interesting to see that the theoretical predictions from chiral *YN* interactions and the two-body result from the phenomenological analysis match so well. Nonetheless,

TABLE I. Partial-wave contributions to $U_\Lambda(k=0)$ (in MeV) at $k_F = 1.35$ fm^{-1}. Results are presented for the SMS *YN* interactions at different chiral orders and with different cutoffs [1] and, in addition, for the NLO13(500) [38] and NLO19(500) [39] interactions. For reference, selected results based on the gap choice are included too.

	$^1S_0$	$^3S_1 + {}^3D_1$	$^3P_0$	$^1P_1$	$^3P_1$	$^3P_2 + {}^3F_2$	Total
SMS LO(700)	−13.9	−28.2	−1.0	0.7	1.0	−0.8	−42.4
SMS NLO(500)	−15.7	−25.6	0.4	4.5	2.0	−3.2	−37.7
SMS NLO(550)	−15.0	−24.5	0.5	2.5	1.5	−4.1	−39.3
SMS NLO(600)	−12.5	−20.2	0.4	1.0	1.5	−4.0	−34.0
SMS N^{2}LO(500)	−16.2	−24.8	0.3	2.9	0.6	−3.2	−41.2
SMS N^{2}LO(550)^a	−15.2	−26.9	0.1	1.2	0.9	−4.9	−45.8
SMS N^{2}LO(550)^b	−15.1	−27.3	0.4	1.5	1.6	−3.4	−43.4
SMS N^{2}LO(600)	−15.3	−25.4	0.2	1.6	1.0	−5.0	−44.1
NLO13(500)	−15.3	−18.9	0.9	0.2	1.6	−1.3	−33.1
NLO19(500)	−13.5	−28.7	0.9	0.3	1.6	−1.2	−40.9
SMS LO(700) gap	−12.1	−24.8	−0.9	0.7	1.0	−0.7	−37.0
SMS NLO(500) gap	−15.2	−22.2	0.5	5.0	2.1	−3.0	−32.9
SMS N^{2}LO(550) gap	−15.6	−20.8	0.4	3.3	0.6	−3.0	−35.9
NLO13(500) gap	−14.7	−13.7	1.0	0.3	1.6	−1.2	−27.0
NLO19(500) gap	−12.0	−27.1	1.0	0.3	1.7	−1.2	−37.5

TABLE II. Partial-wave contributions to $U_\Lambda(k=0)$ (in MeV) in symmetric nuclear matter for $\rho/\rho_0 = (0.5, 1.0, 2.0)$, corresponding to Fermi momenta $k_F = (1.07, 1.35, 1.7)$ fm^{-1}.

	ρ/ρ_0	$^1S_0$	$^3S_1+{}^3D_1$	$^3P_0$	$^1P_1$	$^3P_1$	$^3P_2+{}^3F_2$	S waves	P waves	D waves	Total
SMS LO(700)	0.5	−8.1	−16.9	−0.4	0.2	0.3	−0.3	−25.0	−0.2	−0.1	−25.2
	1.0	−13.9	−28.2	−1.0	0.7	1.0	−0.8	−42.1	−0.2	−0.2	−42.4
	2.0	−23.3	−44.6	−2.4	1.8	2.9	−1.9	−68.2	0.3	−0.9	−68.6
SMS NLO(550)	0.5	−9.1	−17.0	0.1	0.7	0.5	−1.4	−26.1	−0.1	−0.1	−26.2
	1.0	−15.0	−24.5	0.5	2.5	1.5	−4.1	−39.6	0.4	−0.2	−39.3
	2.0	−24.1	−26.6	1.8	8.4	4.7	−11.3	−50.8	3.6	−0.8	−48.0
SMS N^{2}LO(550)^a	0.5	−9.2	−18.2	−0.0	0.3	0.2	−1.8	−27.4	−1.3	−0.3	−28.9
	1.0	−15.2	−26.9	0.1	1.2	0.9	−4.9	−42.0	−2.6	−1.1	−45.8
	2.0	−24.2	−31.8	0.6	4.9	3.4	−12.3	−55.5	−3.3	−4.4	−63.9
SMS N^{2}LO(550)^b	0.5	−9.2	−18.3	0.1	0.4	0.5	−1.3	−27.4	−0.4	−0.3	−28.0
	1.0	−15.1	−27.3	0.4	1.5	1.6	−3.4	−42.4	0.1	−1.1	−43.4
	2.0	−24.0	−33.0	1.6	5.7	5.7	−8.5	−56.7	4.7	−4.4	−56.9
NLO13(500)	0.5	−9.3	−15.3	0.2	0.1	0.5	−0.5	−24.6	0.3	−0.1	−24.3
	1.0	−15.3	−18.9	0.9	0.2	1.6	−1.3	−34.3	1.5	−0.2	−33.1
	2.0	−22.8	0.3	3.5	0.8	4.9	−3.5	−22.9	5.7	−0.8	−17.9
NLO19(500)	0.5	−8.7	−18.3	0.2	0.1	0.5	−0.5	−27.0	0.4	−0.1	−26.6
	1.0	−13.5	−28.7	0.9	0.3	1.6	−1.2	−42.3	1.5	−0.2	−40.9
	2.0	−15.6	−36.5	3.6	0.8	5.0	−3.3	−52.5	6.1	−0.8	−47.2

one should keep in mind that contributions from three-body forces are in general scheme dependent. However, within the Weinberg scheme they can be made consistent with the two-body forces using gradient flow regularization [79]. Such work is underway by the LENPIC Collaboration.

For testing purposes, we performed selected calculations with the gap choice. With that choice for the energy in the intermediate state, the single-particle potential U_Λ at ρ_0 is 3 to 7 MeV less attractive, well in line with earlier observations [63]. Also, our results with the gap choice agree within 1.2 MeV with the ones reported in Ref. [1], which utilized a parametrization of U_N results for the Argonne AV18 NN potential [80], provided in Ref. [81]. On the other hand, our result for NLO13(500) with continuous choice is clearly different from that in Ref. [48]. However, in that work only an NLO NN potential has been used. Potentials up to that order of the chiral expansion tend to be too repulsive for higher momenta/energies [48]. Still, the comparison illustrates that the nucleon single-particle potential can affect $U_Y(k=0)$. That said, when using the N^{3}LO NN potentials from EM or the AV18 NN, we obtain results for U_Y very similar to the calculation with the SMS N^{4}LO$^+$ NN interaction.

We want to remind the reader that at LO only a very basic description of the YN interaction can be obtained [1]. We include the corresponding results primarily for completeness and because they enter into the uncertainty estimate.

Let us now discuss the results in Table I in detail. Obviously, there is a sizable variation in the contribution from the $^3S_1-{}^3D_1$ partial wave, within the SMS potentials but also in comparison to NLO13 and NLO19. It is in the order of 25%. The $^1S_0$ contributions vary in the order of 10%. There are also noticeable variations in the P-wave contributions. As explained in the Introduction, the P waves have been determined differently in the SMS YN potentials and in NLO13 and NLO19. This is clearly reflected in the results in Table I. While there is some variation in the P-wave contributions for the SMS potentials, there are more drastic differences to those for NLO13 and NLO19. As one can see, they differ by a factor of 2–3 ($^3P_0$, $^3P_2$) or even by a factor of 5–10 or more ($^1P_1$). In this context, let us mention that calculations with a YN potential derived within covariant chiral EFT [50] predict even larger (and repulsive) P-wave contributions at ρ_0. Note, however, that the study is performed within the Dirac Brueckner-Hartree-Fock approach. Finally, we want to remark that the P-wave interactions of the NLO13 and NLO19 potentials are identical. In contrast, in the case of SMS N^{2}LO(550)^a and N^{2}LO(550)^b the P waves are different while the S-wave interactions are the same. The two variants are the result of different fits to data on the Σ^+p differential cross section [1] and reflect remaining ambiguities in the P-wave contributions.

In Table II, we list again the partial-wave contributions, however, from a different perspective, namely as a function of the density. We restrict ourselves to the SMS potentials with 550 MeV cutoff and NLO13 and NLO19. One can see that the total S-wave contribution clearly dominates U_Λ up to $2\rho_0$. The difference between NLO and N^{2}LO is fairly moderate. The SMS results for the S waves are also similar to that of NLO19.

With regard to the P-wave contributions, those are overall small but they become more relevant with increasing density. Their smallness is partly due to significant cancellations between the individual contributions. Comparing the individual P-wave results for SMS N^{2}LO and NLO with those from NLO13 and NLO19 reveals that there is no clear tendency. This reflects the fact that the ΛN P-wave interactions are only poorly constrained by the existing experimental data. Specifically instructive are the results for the potentials N^{2}LO(550)^a and N^{2}LO(550)^b established by alternative fits to the Σ^-p differential cross section, as already mentioned above. In this

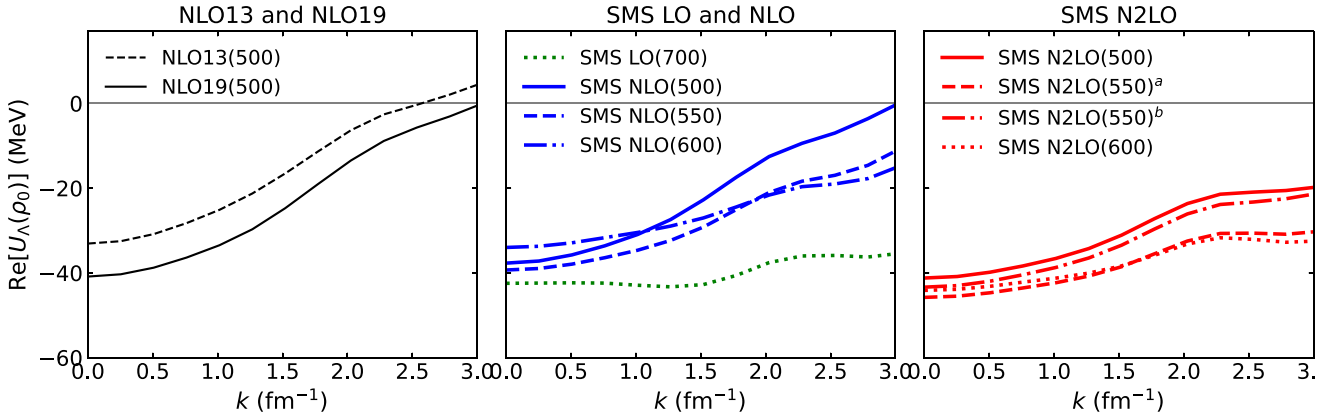

FIG. 4. Momentum dependence of the Λ single-particle potentials in symmetric nuclear matter at ρ_0.

case, even the signs of the total P-wave contribution differ at ρ_0 and $2\rho_0$. A discussion of the impact of the P-wave ambiguities on U_Λ in the context of the YN potentials of the Nijmegen Group can be found in Ref. [63].

Table II reveals that there are also sizable contributions from the D waves, specifically for the N^{2}LO potentials at $2\rho_0$. In order to understand that one has to recall that the contributions at N^{2}LO which arise from two-meson exchange with subleading meson-baryon vertices are relatively large [58]. However, unlike in S and P waves, there are no contact terms in the D waves yet which would counterbalance their effect and/or allow one to reduce possible artifacts from the employed regulator. Such contact terms arise first at N^{3}LO in the chiral expansion. In fact, in this context it is very instructive to look at the corresponding NN results by Hu *et al.* [45]; see their Fig. 1. In the nuclear matter case, the N^{2}LO result clearly deviates from the others and becomes exceptionally attractive with increasing density. When going to N^{3}LO the general trend is restored. It is likely that the same will happen also in the case of the in-medium properties of hyperons. Unfortunately, due to the lack of appropriate scattering data there is no way to extend the YN interaction to N^{3}LO in the foreseeable future.

In Fig. 4 predictions for the momentum dependence of U_Λ at ρ_0 are shown. The momentum dependence of U_Λ from microscopic calculations is often used as a guideline for establishing mean-field models. For example, in Ref. [82], it is argued that the momentum dependence can be a key to solve the hyperon puzzle of neutron stars. Furthermore, the momentum dependence has an impact on the hyperon dynamics in heavy-ion collisions [83].

In the case of the NLO13 and NLO19 potentials, the resulting $U_\Lambda(k)$ rise monotonically with increasing momentum, with a very similar trend. The SMS potentials exhibit a noticeably weaker momentum dependence, except for SMS NLO(500), where the behavior is comparable to that for NLO19(500). Overall, the momentum dependence predicted for the N^{2}LO potentials is more moderate than those for the NLO interactions. The variation of $U_\Lambda(k)$ with the cutoff is of similar magnitude for the SMS NLO and N^{2}LO potentials. Also, in both cases there is a slight increase with increasing momentum.

It is instructive to compare the variation of the momentum dependence with the cutoff to the one observed for U_N based on the N^{4}LO$^+$ potentials; see Fig. 2. It shows what one can expect in a case where the chiral expansion is already well converged and the residual regulator dependence is minimal.

An important quantity related to the momentum dependence is the effective mass, which is sensitive to the energy difference between orbitals of the Λ as considered from mean-field models [84]. The definition of the effective mass of Λ is usually given as

$$\frac{m^*_\Lambda}{m_\Lambda} = \left[1 + 2m_\Lambda \frac{\partial\, \mathrm{Re}U_\Lambda(k)}{\partial k^2}\Big|_{k=0}\right]^{-1}. \tag{6}$$

Since for the considered YN potentials all U_Λ are in line with a k^2 dependence below $k = 1$ fm^{-1}, we evaluate the effective mass as [64]

$$\frac{m^*_\Lambda}{m_\Lambda} = \left[1 + \frac{2m_\Lambda}{k^2}[U_\Lambda(k) - U_\Lambda(0)]\right]^{-1}, \tag{7}$$

with $k = 1$ fm^{-1}. The calculated values are listed in Table III. The values for the SMS N^{2}LO (NLO) potentials are around 0.79–0.86 (0.73–0.83), while those from NLO13 and NLO19 are around 0.7. For the SMS LO potential, $U_\Lambda(k)$ is practically constant for small k and, accordingly, the effective mass is close to 1.0. The SMS NLO and N^{2}LO values are within the hypernuclear constraint, $0.65 < m^*_\Lambda/m_\Lambda < 0.95$ [85].

TABLE III. Normalized effective mass m^*_Λ/m_Λ in symmetric nuclear matter at ρ_0.

	m^*_Λ/m_Λ
SMS LO(700)	1.03
SMS NLO(500)	0.73
SMS NLO(550)	0.79
SMS NLO(600)	0.83
SMS N^{2}LO(500)	0.79
SMS N^{2}LO(550)^a	0.84
SMS N^{2}LO(550)^b	0.79
SMS N^{2}LO(600)	0.86
NLO13(500)	0.69
NLO19(500)	0.71

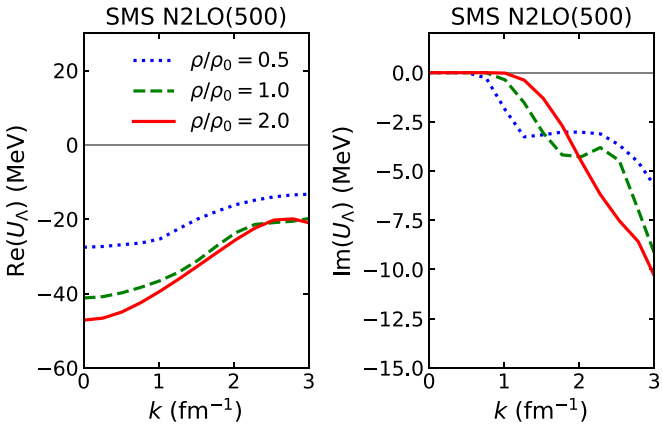

FIG. 5. Momentum dependence of U_Λ in symmetric nuclear matter for $\rho/\rho_0 = (0.5, 1.0, 2.0)$, corresponding to the Fermi momenta $k_F = (1.07, 1.35, 1.7)$ fm^{-1}. The SMS N^{2}LO(500) YN potential is employed.

The variation in the momentum dependence with density is presented in Fig. 5, exemplary for the SMS N^{2}LO(500) potential. We consider densities $\rho = 0.5\rho_0,\ \rho_0,\ 2\rho_0$, corresponding to the Fermi momenta $k_F = (1.07, 1.35, 1.7)$ fm^{-1}. For the Λ single-particle potential, the curvature around $k = 0$ fm^{-1} remains essentially unchanged with increasing density. This behavior means that the Λ effective mass decreases as the density increases, similar to the NLO13 results [48]. The imaginary part of U_Λ is also shown in Fig. 5. As one can see the actual momentum dependence changes noticeably with increasing density.

Finally, in Fig. 6 we show the density dependence of U_Λ for SNM. For the SMS interactions with a cutoff of 500 MeV, and also for NLO13 and NLO19, U_Λ reaches a minimum in the considered density range. In the case of NLO13 there is even a pronounced rise from around $1.5\rho_0$ onwards, while a slower variation with density is seen for the other interactions. As known from the work of Gerstung *et al.*, U_Λ for NLO13 eventually changes sign and becomes repulsive around $2.5\rho_0$ [19]. The origin of the strikingly different behavior of the U_Λ results for NLO13 and NLO19 has been thoroughly discussed in Ref. [39]. It is a consequence of noticeable differences in the strength of the ΛN-ΣN transition potential between the two sets of YN interactions. Broadly speaking, a larger (smaller) channel-coupling strength leads to a less attractive (more attractive) result for U_Λ, even when the corresponding YN scattering results, including the ΛN-ΣN transition cross sections, are identical. The sensitivity of U_Λ to the ΛN-ΣN transition strength has been known for a long time [86–88]. For a complementary demonstration of coupled-channel effects on the in-medium properties of the Λ in the context of the NLO13 YN potential, we refer the reader to the work of Kohno [55]. As likewise discussed in Ref. [39], the actual strength of the transition potential is closely interrelated with possible contributions from three-body forces. Anyway, regarding the SMS NLO and N^{2}LO interactions with larger cutoffs, their trends are still similar to that of the potentials with 500 MeV but, of course, the minimum of U_Λ will be reached at somewhat higher density.

C. Σ in symmetric nuclear matter

Results for the total value and the partial-wave decomposition of the Σ single-particle potential at ρ_0 are listed in Table IV. As one can see, only the SMS LO interaction predicts a small repulsion, while the SMS NLO and N^{2}LO potentials yield an attractive Σ potential at ρ_0. The continuous choice results are around 10 MeV more attractive compared to those for the gap choice. Also, our own gap choice results are slightly more attractive compared to the initial results reported in Ref. [1]. But one has to keep in mind that the calculation in Ref. [1] is based on a finite ϵ in the Bethe-Goldstone equation (1), while now U_Σ is calculated exactly by taking the $\epsilon \to 0$ limit.

NLO13 as well as NLO19 yield a repulsive U_Σ at ρ_0. The primary reason for the difference is that the contribution from the $^3S_1 - {}^3D_1$ partial wave with isospin $I = 3/2$ is noticeably more repulsive than that of the SMS YN potentials. This can be more clearly seen from Table V, where the isospin decomposition is listed. A reduction of the interaction strength in that channel has become necessary due to constraints from

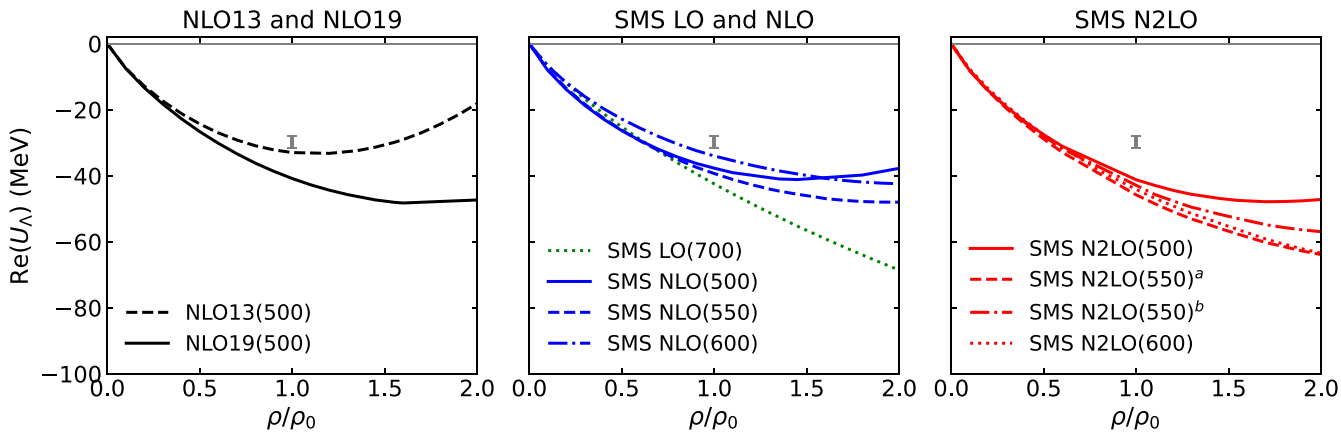

FIG. 6. Density dependence of the Λ single-particle potential in symmetric nuclear matter. The bar symbolizes the quasiempirical value [77].

TABLE IV. Partial-wave contributions to the real part of $U_\Sigma(k=0)$ (in MeV) at ρ_0.

	$^1S_0$	$^3S_1+{}^3D_1$	$^3P_0$	$^1P_1$	$^3P_1$	$^3P_2+{}^3F_2$	Total
SMS LO(700)	−3.3	8.0	−1.0	−0.3	−0.4	−1.8	1.0
SMS NLO(500)	−3.4	−7.4	0.8	0.4	1.7	−1.5	−9.8
SMS NLO(550)	−2.7	−4.6	0.8	−0.5	0.6	−4.5	−11.3
SMS NLO(600)	−2.4	−3.1	0.7	−1.0	0.5	−5.2	−10.9
SMS N^{2}LO(500)	−5.9	−3.2	1.0	0.6	0.8	0.3	−7.8
SMS N^{2}LO(550)^a	−3.4	−4.9	0.5	−0.8	1.0	−1.6	−10.3
SMS N^{2}LO(550)^b	−3.5	−4.9	0.8	−3.3	1.5	−0.4	−11.0
SMS N^{2}LO(600)	−3.2	−5.3	0.6	−2.7	1.2	−2.0	−12.7
NLO13(500)	−4.9	6.4	1.3	0.2	1.2	0.2	3.7
NLO19(500)	−4.4	13.1	1.3	0.2	1.2	0.2	11.2
SMS LO(700) gap	−2.3	14.1	−1.0	−0.2	−0.4	−1.6	8.3
SMS NLO(500) gap	−2.7	−1.3	0.8	0.5	1.7	−1.2	−2.4
SMS N^{2}LO(500) gap	−5.4	6.2	1.0	0.6	0.7	0.6	2.8
NLO13(500) gap	−4.3	16.5	1.4	−0.0	1.1	0.2	14.6
NLO19(500) gap	−3.8	21.2	1.3	−0.1	1.1	0.1	19.7

recent J-PARC E40 data on Σ^+p scattering [43]. The YN potentials NLO13 and NLO19 overshoot those data [1]. In fact, other YN potentials, like the FSS and fss2 interactions derived within the constituent-quark model by Fujiwara *et al.* [89], which predict a repulsive U_Σ at ρ_0, likewise overestimate the cross section of the J-PARC experiment [43]. In contrast, YN potentials like ESC16 [76] by the Nijmegen group that predict Σ^+p cross sections close to those of the SMS YN potentials in the energy region of the J-PARC E40 data (cf. Fig. 3 in that reference) yield likewise a slightly attractive U_Σ. In this context let us mention that preliminary results on the Σ^+p correlation function by the ALICE Collaboration point also to a somewhat weaker Σ^+p interaction in the $^3S_1$ partial wave [90].

At the moment, it remains unclear to us how the constraints provided by the J-PARC data for the Σ^+p interaction can be reconciled with a strongly repulsive U_Σ in the order of 10–50 MeV as advocated in Ref. [77]. Certainly, there can be additional and repulsive contributions from three-body forces, of similar magnitude as expected for U_Λ. Indeed, a corresponding calculation, based on the ΛNN and ΣNN three-body forces introduced in Ref. [19] as a possible solution of the hyperon puzzle, suggests that those contributions are repulsive and could be in the order of 10 to 20 MeV [91]. Then one would come already close to or would be even in agreement with the values inferred from phenomenological potentials. On the other hand, the large spread in the values deduced from various phenomenological analyses of data on Σ^- atoms and $(\pi^-, K^+)\Sigma$ spectra [92–96] discloses that there is a sizable model dependence in such studies. Therefore, one might question whether those potential parameters should be straightforwardly compared with results for U_Σ from a G-matrix calculation. After all, due to the complicated spin-isospin structure of the ΣN interaction, where some of the relevant S waves are attractive and others repulsive, and the coupling to ΛN, the situation is rather complex and it remains unclear to what extent that can be captured by a simple Woods-Saxon form.

For completeness we include in Table V the isoscalar and vector decomposition of U_Σ [77]:

$$U_\Sigma = \left(U_0^\Sigma + \frac{1}{A}\,U_1^\Sigma\,\boldsymbol{T}_A\cdot\boldsymbol{t}_\Sigma\right), \tag{8}$$

where $\boldsymbol{t}_\Sigma$ is the Σ isospin operator and $\boldsymbol{T}_A$ is the nuclear isospin operator with z projection $(Z-N)/2$. The isoscalar U_0^Σ and isovector U_1^Σ components are evaluated by $U_\Sigma^0 = U_{\frac{3}{2}} + U_{\frac{1}{2}}$ and $U_\Sigma^1 = U_{\frac{3}{2}} - 2U_{\frac{1}{2}}$. We note that the isoscalar component is identical to the total value of U_Σ in SNM. The

TABLE V. Partial-wave contributions to $\mathrm{Re}\,U_\Sigma(k=0)$ (in MeV). Total results for the isoscalar (U_Σ^0) and isovector (U_Σ^1) decomposition according to Eq. (8) are given as well. The column on the very right is the conversion width in nuclear matter, $\Gamma_\Sigma = -2\,\mathrm{Im}\,U_\Sigma(k=0)$. Same description of interactions as in Table I.

	Isospin $I=1/2$			Isospin $I=3/2$					
	$^1S_0$	$^3S_1+{}^3D_1$	P	$^1S_0$	$^3S_1+{}^3D_1$	P	$\mathrm{Re}\,U_\Sigma^0$	$\mathrm{Re}\,U_\Sigma^1$	Γ_Σ
SMS LO(700)	7.1	−16.7	−1.9	−10.4	24.7	−1.5	1.0	38.3	21.3
SMS NLO(550)	8.0	−25.0	−0.3	−10.7	20.3	−3.4	−11.3	43.1	30.1
SMS N^{2}LO(550)^a	7.5	−24.9	3.4	−11.0	20.0	−4.4	−10.3	35.0	34.0
SMS N^{2}LO(550)^b	7.5	−24.8	3.6	−11.0	20.0	−5.0	−11.0	33.6	30.4
NLO13(500)	6.2	−26.2	3.7	−11.1	32.5	−0.8	3.7	55.8	30.6
NLO19(500)	6.0	−19.5	3.8	−10.4	32.7	−0.8	11.2	43.2	22.3

TABLE VI. Partial-wave contributions to $\mathrm{Re}\,U_\Sigma(k=0)$ (in MeV) in SNM for $\rho/\rho_0 = (0.5, 1.0, 2.0)$, corresponding to the Fermi momenta $k_F = (1.07, 1.35, 1.7)$ fm^{-1}. Same description of interactions as in Table I.

	ρ/ρ_0	$^1S_0$	$^3S_1+{}^3D_1$	$^3P_0$	$^1P_1$	$^3P_1$	$^3P_2+{}^3F_2$	S waves	P waves	D waves	Total
SMS LO(700)	0.5	−2.4	0.6	−0.5	−0.1	−0.3	−0.7	−1.8	−1.5	−0.1	−3.4
	1.0	−3.3	8.0	−1.0	−0.3	−0.4	−1.8	4.8	−3.5	−0.2	1.0
	2.0	−3.3	28.8	−2.0	−0.8	−0.2	−4.2	25.6	−7.3	−0.6	17.4
SMS NLO(550)	0.5	−2.6	−5.7	0.2	−0.2	0.1	−1.6	−8.2	−1.6	−0.1	−9.9
	1.0	−2.7	−4.6	0.8	−0.5	0.6	−4.5	−7.3	−3.6	−0.2	−11.3
	2.0	−1.1	4.8	3.0	−0.9	2.4	−12.1	3.8	−7.6	−0.8	−4.7
SMS N2LO(550)[a]	0.5	−3.0	−6.2	0.1	−0.4	0.2	−0.7	−9.1	−0.8	−0.2	−10.2
	1.0	−3.4	−4.9	0.5	−0.8	1.0	−1.6	−8.2	−0.9	−0.9	−10.3
	2.0	−2.0	1.8	2.1	−1.6	4.0	−2.1	0.2	2.4	−3.5	−1.5
SMS N2LO(550)[b]	0.5	−3.0	−6.1	0.2	−1.2	0.3	−0.3	−9.1	−1.0	−0.2	−10.4
	1.0	−3.5	−4.9	0.8	−3.3	1.5	−0.4	−8.2	−1.4	−0.9	−11.0
	2.0	−2.1	3.1	3.1	−8.2	5.6	1.0	1.4	1.5	−3.6	−1.1
NLO13(500)	0.5	−3.7	−2.4	0.3	0.0	0.3	−0.1	−6.1	0.5	−0.1	−5.6
	1.0	−4.9	6.4	1.3	0.2	1.2	0.2	1.6	2.8	−0.2	3.7
	2.0	−4.3	43.2	5.2	1.1	4.2	2.1	39.2	12.5	−0.7	50.9
NLO19(500)	0.5	−3.6	0.6	0.3	0.0	0.3	−0.1	−3.0	0.6	−0.1	−2.5
	1.0	−4.4	13.1	1.3	0.2	1.2	0.2	8.8	2.9	−0.2	11.2
	2.0	−2.6	63.1	5.3	1.3	4.2	2.6	60.6	13.4	−0.5	73.1

isovector part is smaller than the phenomenological value listed in Refs. [77,97]. However, also here one has to be cautious with a direct comparison; see the discussion above.

The partial-wave breakdown for different densities is presented in Table VI. The SMS NLO and N^{2}LO potentials yield similar S-wave contributions to U_Σ. They differ considerably from those by NLO13 and NLO19, due to the already mentioned difference in the $I=3/2$ $^3S_1-{}^3D_1$ channel. For P waves, there are again drastic differences in the results for individual partial waves by the different potentials. In some cases the contributions are fairly large like those in the $^3P_2-{}^3F_2$ by the SMS NLO potential or in the $^1P_1$ by the N^{2}LO(550)^b potential. Again, like in case of U_Λ, there are cancellations between the individual P-wave contributions. Due to that, for the two N^{2}LO potentials the total P-wave contributions are almost the same, but they differ noticeably from those for SMS NLO and for the NLO13 and NLO19 potentials. Finally, there is a dramatic increase of the D-wave contribution to U_Σ at $2\rho_0$ in the case of the SMS N^{2}LO potentials. The reasons for that are the same as already discussed for U_Λ in the preceding subsection.

Figure 7 provides the momentum dependence of the Σ single-particle potential in SNM at ρ_0. The real and imaginary part of U_Σ is shown. All SMS potentials predict a quite moderate momentum dependence for low k values. A more noticeable variation occurs only for momenta around $k = 1.5$ fm^{-1}. Overall the results for the SMS NLO and N^{2}LO potentials are very similar. Also the variation with the cutoff is very similar.

Results of $U_\Sigma(k)$ for different densities are shown in Fig. 8, exemplary for the SMS N^{2}LO(500) potential. Overall, the Σ single-particle potential becomes more repulsive with increasing density. Also, the momentum dependence near $k = 0$ fm^{-1} gets more pronounced as density increases while its behavior above $k = 1$ fm^{-1} varies strongly with the density. The imaginary part becomes noticeably larger as density increases, indicating that Σ hyperons are more likely to convert into Λ hyperons at higher density and momenta. The imaginary part of U_Σ is related to the conversion (or spreading) width inside nuclear matter, $\Gamma_\Sigma = -2\,\mathrm{Im}\,U_\Sigma(k=0)$. Our result for SMS N^{2}LO(500), shown in Fig. 8, corresponds to $\Gamma_\Sigma = 34$ MeV at ρ_0. This value is consistent with the ones reported for other YN potentials [65,98]. Some results for other chiral YN potentials are listed in Table V.

Figure 9 shows the density dependence of the Σ single-particle potential in SNM. The SMS NLO and N^{2}LO potentials predict an attractive U_Σ throughout, except for the potentials with a cutoff of 500 MeV where U_Σ turns to repulsion at around $1.5\rho_0$. The results for NLO13 and NLO19 are radically different. Here U_Σ becomes repulsive already at lower densities and then the repulsion increases rapidly with density. As already discussed above, the different behavior is a consequence of the constraints by the J-PARC Σ^+p data [43] on the ΣN interaction in the $I = 3/2$ channel that have been taken into account in the SMS YN potentials.

D. Λ and Σ in pure neutron matter

The dependence of U_Y on the momentum for PNM is presented in Fig. 10, for Λ, Σ^+, Σ^0, and Σ^-, using the SMS N^{2}LO(500) potential. For all cases, U_Y exhibits a fairly weak momentum dependence, similar to that observed in the SNM case. Remarkably, U_{Σ^+} is larger than U_{Σ^-}, for $\rho \geqslant \rho_0$, in contrast to the NLO13 results [48,55]. This is the consequence of the different isospin dependence of the SMS ΣN potential, i.e., the weaker $I = 3/2$ repulsion imposed by the J-PARC E40 data [43], as already seen in the SNM calculation; cf. Table V.

In Fig. 11 the density dependence of the hyperon single-particle potentials in PNM is presented. With regard to the Λ, the SMS NLO and N^{2}LO results exhibit a steady increase of the attraction with density, whereas those from NLO13 and

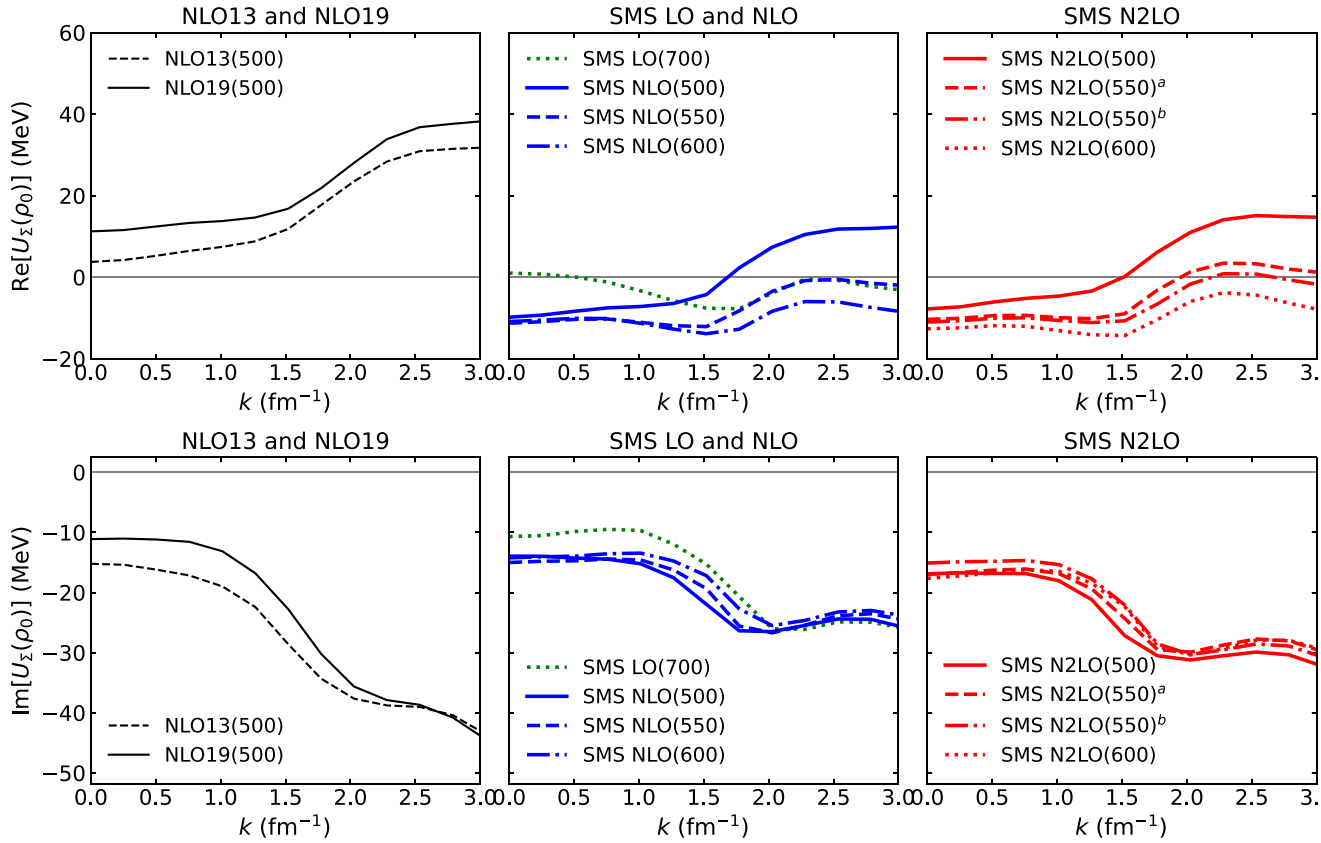

FIG. 7. Momentum dependence of the Σ single-particle potential in symmetric nuclear matter at ρ_0. Both real and imaginary parts are shown.

NLO19 become noticeably less attractive from around ρ_0 onward. Nevertheless the difference between the SNM and PNM results are small for the Λ, since it is an isoscalar particle.

In contrast, the isospin $I = 1$ hyperon Σ is strongly affected by the relative fraction of protons and neutrons in nuclear matter. The $\Sigma^- n$ system has isospin $I = 3/2$. The corresponding interaction is identical to the one for $\Sigma^+ p$ when isospin-breaking effects are disregarded and predominantly repulsive. However, in the case of the SMS YN potentials the repulsion is significantly reduced in comparison to NLO13 and NLO19, due to their adjustment to the new $\Sigma^+ p$ data, as already mentioned. As a result, the corresponding Σ^- single-particle potential is not strongly repulsive anymore.

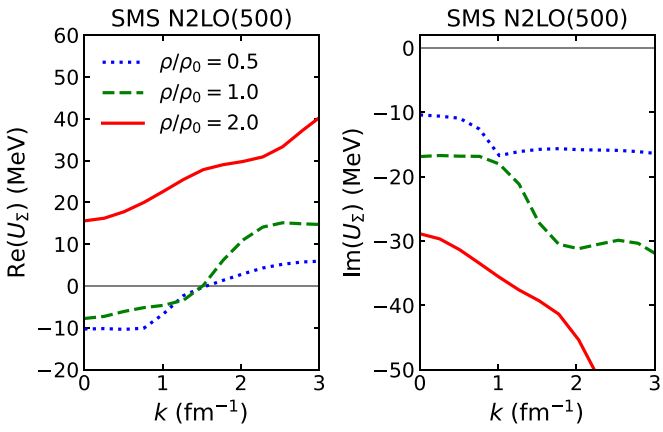

FIG. 8. Momentum dependence of U_Σ in symmetric nuclear matter for $\rho/\rho_0 = (0.5, 1.0, 2.0)$, corresponding to the Fermi momenta $k_F = (1.07, 1.35, 1.7)$ fm^{-1}. The SMS N^{2}LO(00) YN potential is employed.

IV. UNCERTAINTY ESTIMATE

In this section, we provide an uncertainty estimate for the hyperon single-particle potentials at $k = 0$, i.e., for the quantity that is associated with the binding energy of hyperons in infinite nuclear matter. In particular, we estimate and discuss the truncation error in the chiral expansion, following the method proposed by Epelbaum, Krebs, and Meißner (EKM) [53,99]. It combines information about the expected size and actual size of higher-order corrections. It can be applied to any observable X which has been evaluated up to a specific order i in the chiral expansion, $X^{(i)}$. The concrete expressions for the corresponding uncertainty $\delta X^{(i)}$ are [54]

$$\begin{aligned}
\delta X^{\mathrm{LO}} &= Q^2 |X^{\mathrm{LO}}|, \\
\delta X^{\mathrm{NLO}} &= \max(Q^3 |X^{\mathrm{LO}}|, Q|X^{\mathrm{NLO}} - X^{\mathrm{LO}}|), \\
\delta X^{\mathrm{N^2LO}} &= \max\big(Q^4 |X^{\mathrm{LO}}|, Q^2 |X^{\mathrm{NLO}} - X^{\mathrm{LO}}|, \\
&\qquad Q|X^{\mathrm{N^2LO}} - X^{\mathrm{NLO}}|\big),
\end{aligned} \tag{9}$$

with the additional constraint for the theoretical uncertainties at LO and NLO to have at least the size of the actual

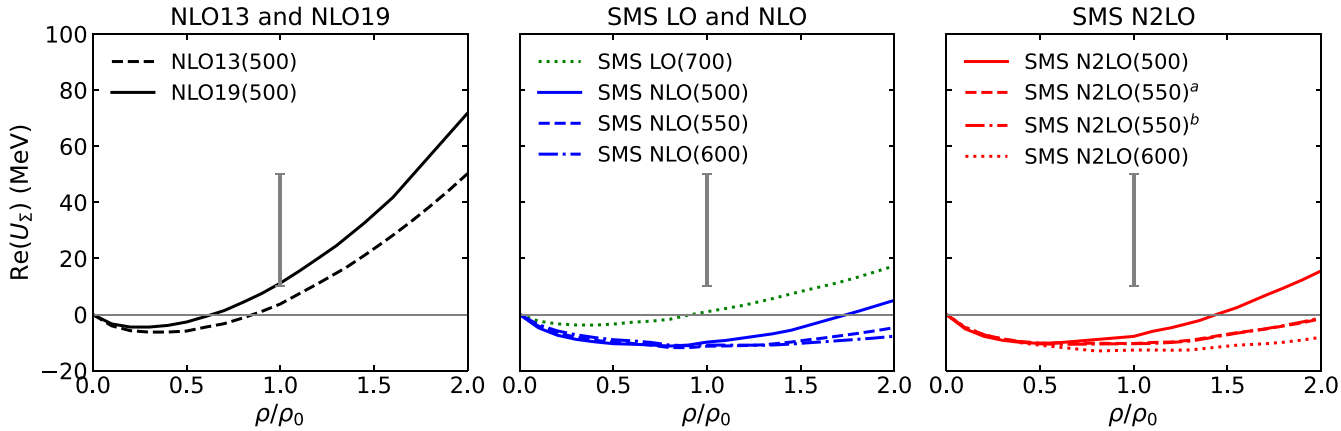

FIG. 9. Density dependence of the Σ single-particle potential in symmetric nuclear matter. The bar indicates results from phenomenological analyses [77].

higher-order contributions [53]. Here, Q represents the expansion scale in the chiral expansion, which is given by $Q \in \{p/\Lambda_b, M_\pi/\Lambda_b\}$, where p is the typical momentum of the baryons, M_π is the pion mass, and Λ_b is the breakdown scale of the chiral expansion. This method has been already applied to nuclear matter properties in the work by Hu *et al.* [45]. Thereby, the momentum scale p has been identified with the Fermi momentum k_F. We adopt the same prescription in our work.

For the breakdown scale we use $\Lambda_b = 480$ and 600 MeV for SNM and PNM, respectively. This choice was guided by the Bayesian analysis of nuclear matter properties by Hu *et al.* [46], which suggested a breakdown scale of 480 MeV for SNM and 660–720 MeV for PNM. In the initial study by Hu *et al.* [45] with the EKM method, $\Lambda_b = 600$ MeV has been used. The breakdown scale in the original work by EKM was estimated to be around $\Lambda_b = 400$–600 MeV [54], based on results for NN phase shifts and scattering observables. The typical values of Q are 0.55 and 0.69 at ρ_0 and $2\rho_0$ in SNM, respectively. For comparison, in the study of the uncertainty for light Λ hypernuclei a scale of $Q = 0.4$ was found appropriate [100]. As pointed out in Ref. [54], such a simple estimation of the theoretical uncertainty does not provide a statistical interpretation. Nonetheless, the procedure can be interpreted in a Bayesian sense [101].

In Fig. 12, the uncertainty estimate for the density dependence of $U_\Lambda(k = 0)$ in SNM is shown. We selected the SMS LO(700), SMS NLO(550), and SMS N^{2}LO(550)^b YN potentials as an exemplary set. The other cutoffs of 500 and 600 MeV result in very similar uncertainty bands for the SNM calculations. The upper limits of the LO and NLO uncertainty bands at ρ_0 touch the quasiempirical value of $U_\Lambda \approx -30$ MeV. In contrast, the N^{2}LO band underestimates it. The actual estimates at ρ_0 are

$$U_\Lambda^{\rm NLO}(\rho_0) = -39.3 \pm 7.0 \text{ MeV},$$
$$U_\Lambda^{\rm N^2LO}(\rho_0) = -43.5 \pm 3.8 \text{ MeV}. \quad (10)$$

Obviously, the uncertainty is of an order which brings the SMS NLO results (and those of the NLO13 and NLO19 YN potentials) practically in line with the quasiempirical value of U_Λ. An interesting aspect is, of course, that the uncertainty of the NLO result provides also a glimpse on the size of missing YNN three-body forces. The present estimate is compatible with the actual contribution of an effective three-body force evaluated in Ref. [19], established within the

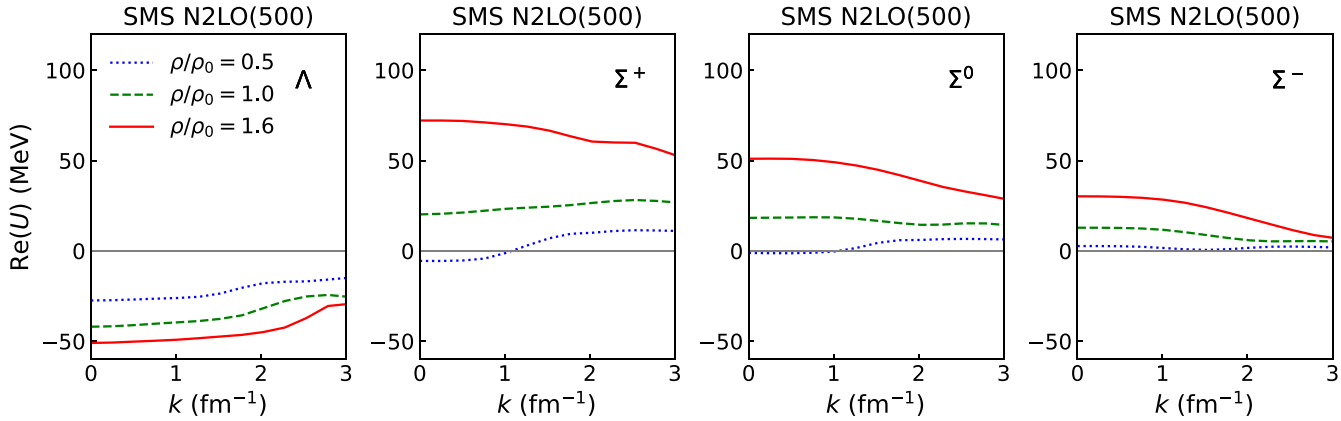

FIG. 10. Momentum dependence of the real part of the single-particle potentials for hyperons in pure neutron matter for different densities $\rho = (0.5, 1.0, 1.6)$, corresponding to the Fermi momenta $k_F = (1.35, 1.7, 2.0)$ fm^{-1}.

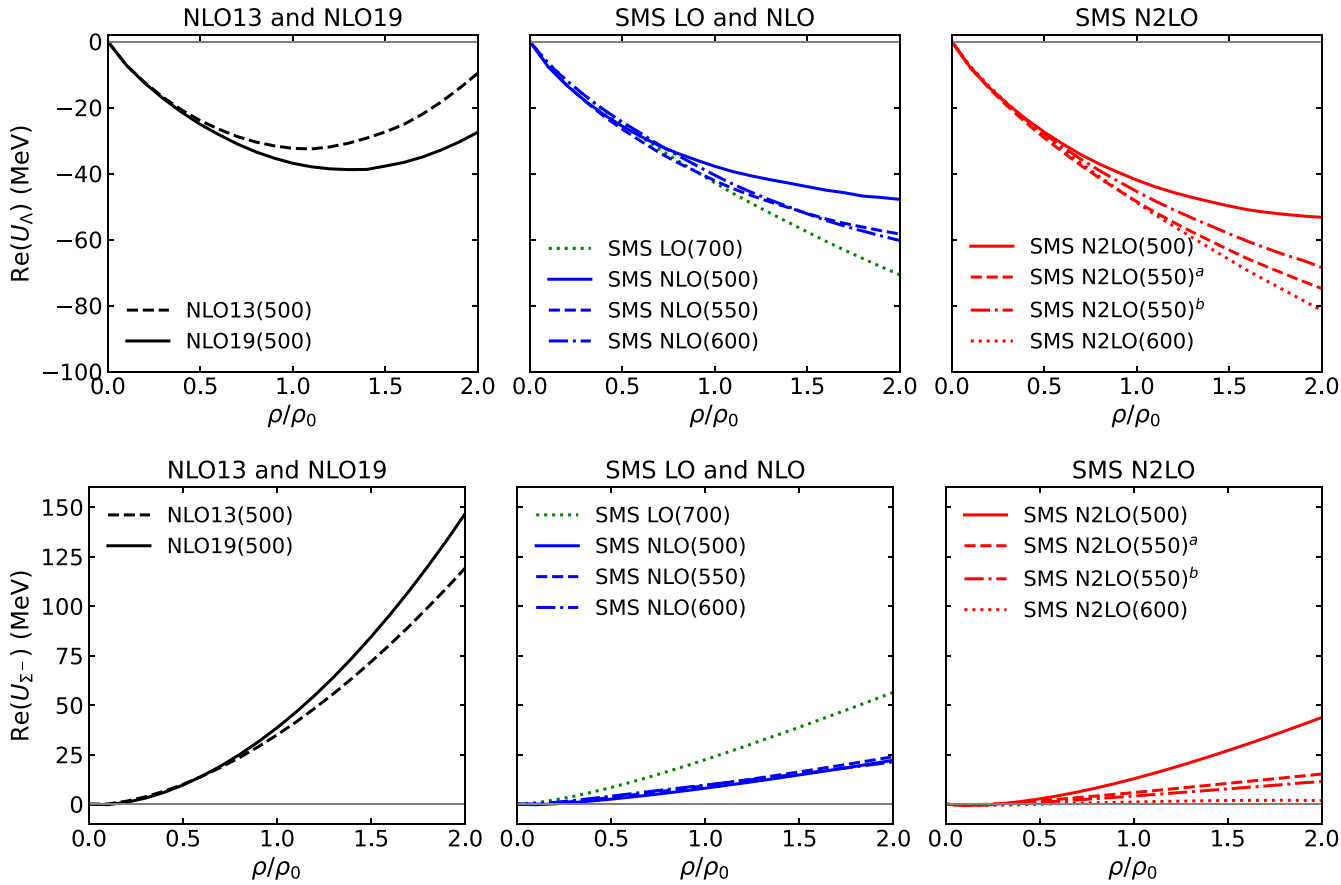

FIG. 11. Density dependence of the Λ (upper panels) and Σ^- (lower panels) single-particle potentials in pure neutron matter.

assumption of decuplet saturation and based on LECs constrained from dimensional scaling arguments. It is also comparable to the value suggested in Ref. [78] within a phenomenological analysis. Comparing the uncertainty estimate with the NLO results for different cutoffs in Table I, one can see that the cutoff variations are noticeably smaller. This confirms again the conclusion that the cutoff variation does not provide a reliable measure for estimating uncertainties, stressed already in earlier studies of nuclear matter [45,102]. Indeed, as emphasized in Ref. [54], in general the residual cutoff dependence underestimates the theoretical uncertainty. Since the calculation at N^2LO is incomplete, i.e., three-body forces are missing, one has to be somewhat cautious with the interpretation of the corresponding result. Strictly speaking,

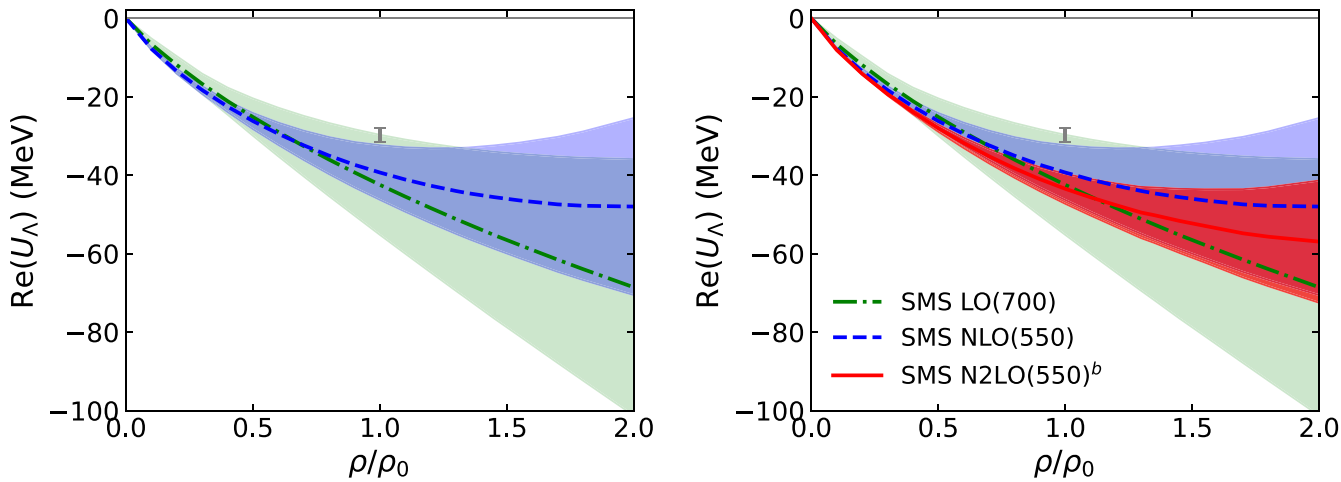

FIG. 12. Uncertainty estimate of the Λ single-particle potentials in symmetric nuclear matter. The SMS NLO and N^2LO interactions with cutoff 550 MeV are employed, while for SMS LO the potential with 700 MeV cutoff is used. The bar symbolizes the quasiempirical value [77].

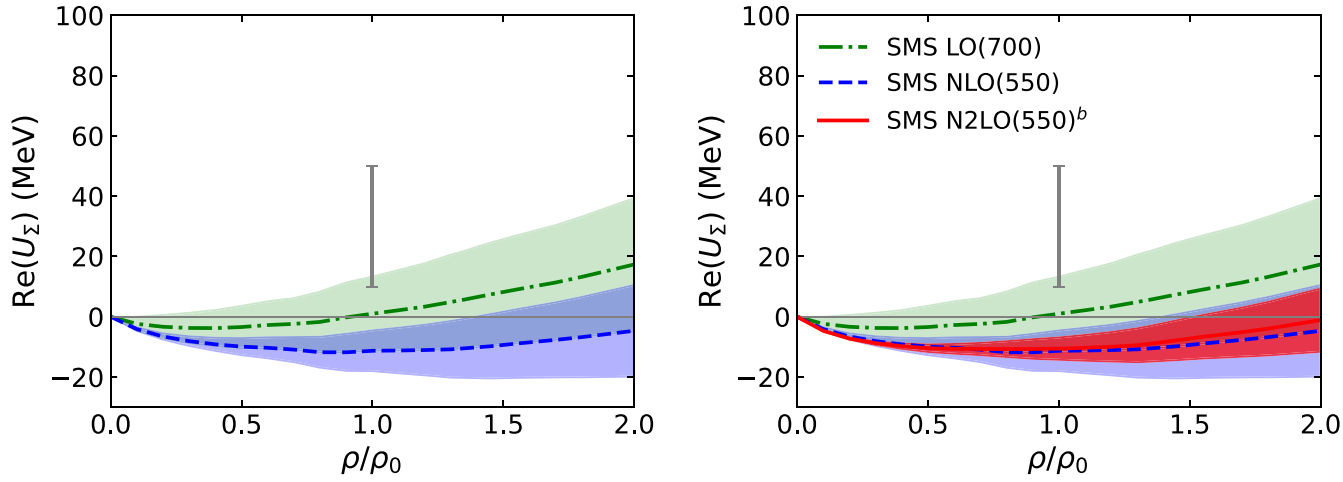

FIG. 13. Same as Fig. 12, but for Σ. The bar indicates results from phenomenological analyses, taken from Ref. [77].

the actual uncertainty is still the one obtained for the result at NLO. This concerns not only the estimate at ρ_0 but also the one at the highest density considered by us. As one can see from Fig. 12, the uncertainty of U_Λ increases rapidly with density and amounts to roughly ±20 MeV at $2\rho_0$.

Additional uncertainties arise due to the issues already discussed in Sec. III B. Since the P-wave interactions in the ΛN system are not directly constrained, only indirectly via $\Sigma^- p$ and $\Sigma^+ p$ differential cross sections and the assumed SU(3) symmetry, their contribution to U_Λ at ρ_0 varies in the order of 4 MeV for the considered chiral YN potentials, cf. Table II, and by almost 10 MeV at $2\rho_0$. In the case of the N^{2}LO calculation even uncertainties in the D waves might become relevant. Actually, in the context of the N^{2}LO potential it is instructive to take a look at the nuclear matter case, where calculations have been performed up to N^{4}LO. There the result at N^{2}LO sticks out from the general trend as being particularly attractive; see Fig. 1 in Ref. [45]. Thus one can speculate that also for the Λ the N^{2}LO result is somewhat exceptional and a fully converged calculation would rather yield values for U_Λ that are close to those obtained for the SMS NLO YN potentials.

Note that other uncertainties, like those associated with the use of the BHF approximation [67–69,103], are not considered here.

The uncertainty estimation for Σ in SNM is presented in Fig. 13. The corresponding uncertainty at ρ_0 is

$$U_\Sigma^{\rm NLO}(\rho_0) = -11.3 \pm 6.7 \text{ MeV},$$
$$U_\Sigma^{\rm N^2LO}(\rho_0) = -10.6 \pm 3.7 \text{ MeV}. \quad (11)$$

The uncertainty bands for the NLO and N^{2}LO potentials are similar because there is not much difference between the results at NLO and N^{2}LO, as can be seen from Fig. 7. Obviously, U_Σ is predicted to be attractive up to $1.5\rho_0$, even when considering the theoretical uncertainty.

In Fig. 14 we show the Σ^- single-particle potential in PNM. The values at ρ_0 in PNM are

$$U_{\Sigma^-}^{\rm NLO}(\rho_0) = 9.4 \pm 7.2 \text{ MeV},$$
$$U_{\Sigma^-}^{\rm N^2LO}(\rho_0) = 4.1 \pm 4.0 \text{ MeV}. \quad (12)$$

Compared to the case of U_Σ in SNM, the N^{2}LO uncertainty band is noticeably larger due to the fact that for a given ρ_0 the Fermi momentum in PNM is larger. Obviously U_{Σ^-} is predominantly repulsive, for the SMS NLO as well as for the N^{2}LO potentials.

We do not show results for Λ in PNM since the uncertainties are very similar to those in SNM, reflecting the isoscalar nature of the Λ hyperon.

We have made some exploratory calculations utilizing a Bayesian approach [104]. Those yield results very similar to the EKM method. Therefore, we postpone a full-fledged Bayesian analysis for the future.

V. SUMMARY AND OUTLOOK

We have investigated the properties of hyperons in nuclear matter within the self-consistent Brueckner-Hartree-Fock approach using the continuous choice for intermediate states. We employed the recently established semilocal momentum-space regularized (SMS) hyperon-nucleon interaction up to next-to-next-to-leading order, enabling a systematic investigation of the order-by-order convergence. We also used the NN interaction by Reinert *et al.* [40], regularized in the same scheme as the hyperon-nucleon potential, to evaluate the nucleon single-particle potential.

The Λ single-particle potentials from the SMS YN interactions turned out to be qualitatively similar to those predicted by the NLO13 and NLO19 interactions, at least up to nuclear matter saturation density. However, overall, the resulting in-medium potentials from the new YN interactions are slightly more attractive, in particular those from the N^{2}LO interaction. This concerns first of all the value of U_Λ at the momentum $k = 0$ MeV, associated with the binding energy of the Λ in infinite nuclear matter, but is reflected also in the momentum dependence. For the Σ case the results for the SMS YN potentials differ noticeably from those for our earlier chiral YN potentials. Specifically, now the single-particle potential in symmetric nuclear matter at the saturation density is even attractive, $U_\Sigma \approx -10$ MeV, while results in the order of $U_\Sigma \approx +10$ MeV are predicted by the NLO13/NLO19 potentials.

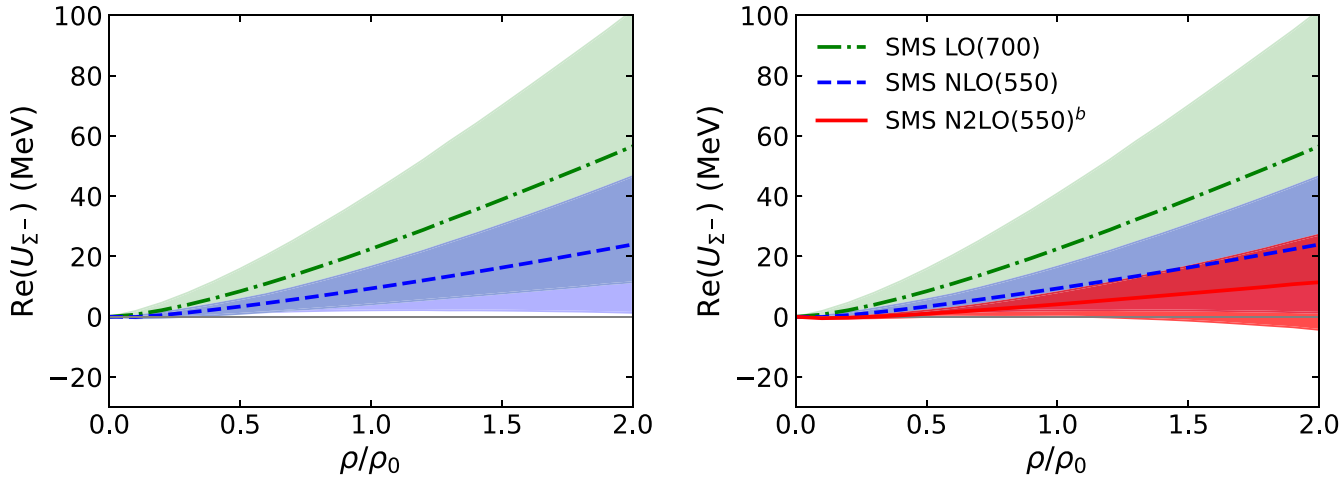

FIG. 14. Uncertainty estimate of the Σ^- single-particle potentials in pure neutron matter.

The reason for the difference is new constraints from Σ^+p and Σ^-p differential cross section data from the J-PARC E40 experiment [41–43], which have been taken into account when the SMS YN potentials have been established.

In the present work we reported also on the first effort to estimate the error due to the truncation in the chiral expansion for the single-particle potentials. Thereby we followed a procedure proposed by Epelbaum, Krebs, and Meißner [54], a simple but efficient method which combines information about the expected size and the actual size of higher-order corrections. The estimated uncertainty relevant for the Λ is in the order of 7 MeV at nuclear matter saturation density. It is comparable with the difference of the theoretical results for U_Λ at NLO to the usually quoted quasiempirical value of $U_\Lambda \approx -30$ MeV.

The present results at N^{2}LO are incomplete because corresponding contributions from leading three-body forces, which arise at that order of the chiral expansion, have not been taken into account. Indeed, the uncertainty estimate for the NLO result allows a first rough conclusion on the actual size of possible contributions from YNN three-body forces. An explicit calculation of their effect is, however, extremely challenging. One needs to solve the Bethe-Faddeev equation [105,106] with chiral three-body forces. So far pertinent investigations in the context of chiral NN [102,107] and YN [18,19] potentials have been limited to an approximation, namely to the application of density-dependent two-body potentials derived from the N^{2}LO three-body force. Such an effective interaction can be obtained by summing one particle over the occupied states in the Fermi sea [74,75,108,109]. In the on-shell approximation the resulting YN (NN) interaction can be expressed in analytical form with operator structures identical to those of free-space YN (NN) interactions; see Ref. [109] for details. This idea has been already exploited by Gerstung *et al.* [19] and they showed that with such an effective three-body force one can not only reproduce the quasiempirical value of U_Λ at ρ_0 but even solve the hyperon puzzle. In principle, one could avoid the on-shell approximation by summing one particle over the occupied states in the Fermi sea numerically. In this case, there would be a much more direct connection between the three-body forces as used in *ab initio* few-body calculations [44] and the ones that enter the G-matrix calculation. Work along this line is left for the future.

ACKNOWLEDGMENTS

We would like to thank J. Hu and I. Vidaña for sharing their results and for fruitful communication, T. Duguet, A. Gal, A. Nogga, and E. Oset for useful discussions, and D. Gerstung for kindly sharing his code with us. This work was supported in part by JST SPRING (Grant No. JPMJSP2110) and by the Grants-in Aid for Scientific Research from JSPS (Grant No. JP25KJ1584), by the European Research Council (ERC) under the European Union's Horizon 2020 research and innovation programme (ERC AdG EXOTIC, Grant Agreement No. 101018170), and the CAS President's International Fellowship Initiative (PIFI) (Grant No. 2025PD0022).

DATA AVAILABILITY

The data that support the findings of this article are not publicly available. The data are available from the authors upon reasonable request.

[1] J. Haidenbauer, U.-G. Meißner, A. Nogga, and H. Le, Hyperonnucleon interaction in chiral effective field theory at next-to-next-to-leading order, Eur. Phys. J. A **59**, 63 (2023).

[2] K. Miyagawa and W. Glöckle, Hypertriton calculation with meson theoretical nucleon-nucleon and hyperon nucleon interactions, Phys. Rev. C **48**, 2576 (1993).

[3] A. Nogga, H. Kamada, and W. Glöckle, The hypernuclei $^4_\Lambda$He and $^4_\Lambda$He: Challenges for modern hyperon nucleon forces, Phys. Rev. Lett. **88**, 172501 (2002).

[4] A. Nogga, Light hypernuclei based on chiral and phenomenological interactions, Nucl. Phys. A **914**, 140 (2013).

[5] J. Haidenbauer, U.-G. Meißner, and A. Nogga, Constraints on the Λ-Neutron interaction from charge symmetry breaking in the ${}^{4}_{\Lambda}$He - ${}^{4}_{\Lambda}$H hypernuclei, Few Body Syst. **62**, 105 (2021).

[6] R. Wirth, D. Gazda, P. Navrátil, A. Calci, J. Langhammer, and R. Roth, *Ab initio* description of p-shell hypernuclei, Phys. Rev. Lett. **113**, 192502 (2014).

[7] R. Wirth and R. Roth, Light neutron-rich hypernuclei from the importance-truncated no-core shell model, Phys. Lett. B **779**, 336 (2018).

[8] H. Le, J. Haidenbauer, U.-G. Meißner, and A. Nogga, Jacobi no-core shell model for *p*-shell hypernuclei, Eur. Phys. J. A **56**, 301 (2020).

[9] H. Le, J. Haidenbauer, U.-G. Meißner, and A. Nogga, *Ab initio* calculation of charge-symmetry breaking in A=7 and 8 Λ hypernuclei, Phys. Rev. C **107**, 024002 (2023).

[10] H. Le, J. Haidenbauer, H. Kamada, M. Kohno, U.-G. Meißner, K. Miyagawa, and A. Nogga, Benchmarking $\mathbf{\Lambda}$NN three-body forces and first predictions for $A = 3 - 5$ hypernuclei, Eur. Phys. J. A **61**, 21 (2025).

[11] F. Hildenbrand, S. Elhatisari, Z. Ren, and U.-G. Meißner, Towards hypernuclei from nuclear lattice effective field theory, Eur. Phys. J. A **60**, 215 (2024).

[12] Y. Yamamoto, T. Motoba, H. Himeno, K. Ikeda, and S. Nagata, Hyperon nucleon and hyperon-hyperon interactions in nuclei, Prog. Theor. Phys. Suppl. **117**, 361 (1994).

[13] E. Hiyama, M. Kamimura, T. Motoba, T. Yamada, and Y. Yamamoto, Three- and four-body cluster models of hypernuclei using the *G*-matrix ΛN interaction: ${}^{9}_{\Lambda}$Be, ${}^{13}_{\Lambda}$C, ${}^{6}_{\Lambda\Lambda}$He and ${}^{10}_{\Lambda\Lambda}$Be, Prog. Theor. Phys. **97**, 881 (1997).

[14] I. Vidaña, A. Polls, A. Ramos, and M. Hjorth-Jensen, Hyperon properties in finite nuclei using realistic YN interactions, Nucl. Phys. A **644**, 201 (1998).

[15] Y. Fujiwara, M. Kohno, and Y. Suzuki, $\Lambda\alpha$, $\sigma\alpha$ and $\xi\alpha$ potentials derived from the SU(6) quark-model baryon-baryon interaction, Nucl. Phys. A **784**, 161 (2007).

[16] I. Vidaña, Single-particle spectral function of the Λ hyperon in finite nuclei, Nucl. Phys. A **958**, 48 (2017).

[17] J. Haidenbauer and I. Vidaña, Structure of single-Λ hypernuclei with chiral hyperon-nucleon potentials, Eur. Phys. J. A **56**, 55 (2020).

[18] J. Haidenbauer, U.-G. Meißner, N. Kaiser, and W. Weise, Lambda-nuclear interactions and hyperon puzzle in neutron stars, Eur. Phys. J. A **53**, 121 (2017).

[19] D. Gerstung, N. Kaiser, and W. Weise, Hyperonnucleon three-body forces and strangeness in neutron stars, Eur. Phys. J. A **56**, 175 (2020).

[20] D. Logoteta, I. Vidaãna, and I. Bombaci, Impact of chiral hyperonic three-body forces on neutron stars, Eur. Phys. J. A **55**, 207 (2019).

[21] I. Vidaña, V. Mantovani Sarti, J. Haidenbauer, D. L. Mihaylov, and L. Fabbietti, Neutron star properties and femtoscopic constraints, Eur. Phys. J. A **61**, 59 (2025).

[22] N. K. Glendenning and S. A. Moszkowski, Reconciliation of neutron star masses and binding of the Λ in hypernuclei, Phys. Rev. Lett. **67**, 2414 (1991).

[23] R. Knorren, M. Prakash, and P. J. Ellis, Strangeness in hadronic stellar matter, Phys. Rev. C **52**, 3470 (1995).

[24] S. Balberg and A. Gal, An effective equation of state for dense matter with strangeness, Nucl. Phys. A **625**, 435 (1997).

[25] S. Nishizaki, T. Takatsuka, and Y. Yamamoto, Hyperon-mixed neutron star matter and neutron stars, Prog. Theor. Phys. **108**, 703 (2002).

[26] S. Weissenborn, D. Chatterjee, and J. Schaffner-Bielich, Hyperons and massive neutron stars: Vector repulsion and SU(3) symmetry, Phys. Rev. C **85**, 065802 (2012); **90**, 019904(E) (2014).

[27] H. Togashi, E. Hiyama, Y. Yamamoto, and M. Takano, Equation of state for neutron stars with hyperons by the variational method, Phys. Rev. C **93**, 035808 (2016).

[28] M. Fortin, S. S. Avancini, C. Providência, and I. Vidaña, Hypernuclei and massive neutron stars, Phys. Rev. C **95**, 065803 (2017).

[29] H. Tong, S. Elhatisari, and U.-G. Meißner, *Ab initio* calculation of hyper-neutron matter, Sci. Bull. **70**, 825 (2025).

[30] Y. Fujimoto, T. Kojo, and L. McLerran, Quarkyonic matter pieces together the hyperon puzzle, arXiv:2410.22758.

[31] L. Tolos and L. Fabbietti, Strangeness in nuclei and neutron stars, Prog. Part. Nucl. Phys. **112**, 103770 (2020).

[32] G. F. Burgio, H. J. Schulze, I. Vidaña, and J. B. Wei, Neutron stars and the nuclear equation of state, Prog. Part. Nucl. Phys. **120**, 103879 (2021).

[33] J. Schaffner-Bielich, *Compact Star Physics* (Cambridge University Press, Cambridge, UK, 2020), p. 8.

[34] I. Vidaña, Neutron stars and the hyperon puzzle, EPJ Web Conf. **271**, 09001 (2022).

[35] K. A. Brueckner, C. A. Levinson, and H. M. Mahmoud, Two-Body forces and nuclear saturation. 1. Central forces, Phys. Rev. **95**, 217 (1954).

[36] K. A. Brueckner and C. A. Levinson, Approximate reduction of the many-body problem for strongly interacting particles to a problem of self-consistent fields, Phys. Rev. **97**, 1344 (1955).

[37] B. D. Day, Elements of the Brueckner-Goldstone theory of nuclear matter, Rev. Mod. Phys. **39**, 719 (1967).

[38] J. Haidenbauer, S. Petschauer, N. Kaiser, U.-G. Meißner, A. Nogga, and W. Weise, Hyperon-nucleon interaction at next-to-leading order in chiral effective field theory, Nucl. Phys. A **915**, 24 (2013).

[39] J. Haidenbauer, U.-G. Meißner, and A. Nogga, Hyperon–nucleon interaction within chiral effective field theory revisited, Eur. Phys. J. A **56**, 91 (2020).

[40] P. Reinert, H. Krebs, and E. Epelbaum, Semilocal momentum-space regularized chiral two-nucleon potentials up to fifth order, Eur. Phys. J. A **54**, 86 (2018).

[41] K. Miwa, *et al.*, Precise measurement of differential cross sections of the $\Sigma^- p \to \Lambda n$ reaction in momentum range 470-650 MeV/c, Phys. Rev. Lett. **128**, 072501 (2022).

[42] K. Miwa, *et al.*, Measurement of the differential cross sections of the $\Sigma^- p$ elastic scattering in momentum range 470 to 850 MeV/c, Phys. Rev. C **104**, 045204 (2021).

[43] T. Nanamura, *et al.*, Measurement of differential cross sections for Σ p elastic scattering in the momentum range 0.44–0.80 GeV/c, PTEP **9**, 093D01 (2022).

[44] H. Le, J. Haidenbauer, U.-G. Meißner, and A. Nogga, Light Λ hypernuclei studied with chiral hyperon-nucleon and hyperon-nucleon-nucleon forces, Phys. Rev. Lett. **134**, 072502 (2025).

[45] J. Hu, Y. Zhang, E. Epelbaum, U.-G Meißner, and J. Meng, Nuclear matter properties with nucleon-nucleon forces up to fifth order in the chiral expansion, Phys. Rev. C **96**, 034307 (2017).

[46] J. Hu, P. Wei, and Y. Zhang, Bayesian truncation errors in equations of state of nuclear matter with chiral nucleon-nucleon potentials, Phys. Lett. B **798**, 134982 (2019).
[47] J. Haidenbauer and U.-G. Meißner, A study of hyperons in nuclear matter based on chiral effective field theory, Nucl. Phys. A **936**, 29 (2015).
[48] S. Petschauer, J. Haidenbauer, N. Kaiser, U.-G. Meißner, and W. Weise, Hyperons in nuclear matter from SU(3) chiral effective field theory, Eur. Phys. J. A **52**, 15 (2016).
[49] D. L. Mihaylov, J. Haidenbauer, and V. Mantovani Sarti, Constraining the p Λ interaction from a combined analysis of scattering data and correlation functions, Phys. Lett. B **850**, 138550 (2024).
[50] R.-Y. Zheng, Z.-W. Liu, L.-S. Geng, J.-N. Hu, and S. Wang, In-medium Λ n interactions with leading order covariant chiral hyperon/nucleon-nucleon forces, Phys. Lett. B **864**, 139416 (2025).
[51] B. Sechi-Zorn, B. Kehoe, J. Twitty, and R. A. Burnstein, Low-Energy Λ–Proton elastic scattering, Phys. Rev. **175**, 1735 (1968).
[52] G. Alexander, U. Karshon, A. Shapira, G. Yekutieli, R. Engelmann, H. Filthuth, and W. Lughofer, Study of the Λ–N system in low-energy Λ–p elastic scattering, Phys. Rev. **173**, 1452 (1968).
[53] E. Epelbaum, H. Krebs, and U.-G. Meißner, Improved chiral nucleon-nucleon potential up to next-to-next-to-next-to-leading order, Eur. Phys. J. A **51**, 53 (2015).
[54] E. Epelbaum, H. Krebs, and U.-G. Meißner, Precision nucleon-nucleon potential at fifth order in the chiral expansion, Phys. Rev. Lett. **115**, 122301 (2015).
[55] M. Kohno, Single-particle potential of the Λ hyperon in nuclear matter with chiral effective field theory NLO interactions including effects of YNN three-baryon interactions, Phys. Rev. C **97**, 035206 (2018).
[56] H. Polinder, J. Haidenbauer, and U.-G. Meißner, Hyperon nucleon interactions: A chiral effective field theory approach, Nucl. Phys. A **779**, 244 (2006).
[57] S. Petschauer and N. Kaiser, Relativistic SU(3) chiral baryon-baryon lagrangian up to order q^2, Nucl. Phys. A **916**, 1 (2013).
[58] E. Epelbaum, W. Glöckle, and U.-G. Meißner, The two-nucleon system at next-to-next-to-next-to-leading order, Nucl. Phys. A **747**, 362 (2005).
[59] J. Haidenbauer, U.-G. Meißner, and A. Nogga, *Ab initio* description of hypernuclei, arXiv:2508.05243.
[60] P. Eckert, P. Achenbach, *et al.*, Chart of hypernuclides—hypernuclear structure and decay data, https://hypernuclei.kph.uni-mainz.de.
[61] S. Petschauer, N. Kaiser, J. Haidenbauer, U.-G. Meißner, and W. Weise, Leading three-baryon forces from SU(3) chiral effective field theory, Phys. Rev. C **93**, 014001 (2016).
[62] A. Reuber, K. Holinde, and J. Speth, Meson exchange hyperon-nucleon interactions in free scattering and nuclear matter, Nucl. Phys. A **570**, 543 (1994).
[63] T. A. Rijken, V. G. J. Stoks, and Y. Yamamoto, Soft core hyperon - nucleon potentials, Phys. Rev. C **59**, 21 (1999).
[64] M. Kohno, Y. Fujiwara, T. Fujita, C. Nakamoto, and Y. Suzuki, Hyperon single particle potentials calculated from SU(6) quark model baryon baryon interactions, Nucl. Phys. A **674**, 229 (2000).
[65] H. J. Schulze, M. Baldo, U. Lombardo, J. Cugnon, and A. Lejeune, Hyperonic nuclear matter in Bruckner theory, Phys. Rev. C **57**, 704 (1998).
[66] I. Vidaña, A. Polls, A. Ramos, M. Hjorth-Jensen, and V. G. J. Stoks, Strange nuclear matter within Bruckner-Hartree-Fock theory, Phys. Rev. C **61**, 025802 (2000).
[67] H. Q. Song, M. Baldo, G. Giansiracusa, and U. Lombardo, Bethe-Brueckner-Goldstone expansion in nuclear matter, Phys. Rev. Lett. **81**, 1584 (1998).
[68] M. Baldo, A. Fiasconaro, H. Q. Song, G. Giansiracusa, and U. Lombardo, High density symmetric nuclear matter in the Bethe-Brueckner-Goldstone approach, Phys. Rev. C **65**, 017303 (2001).
[69] J.-J. Lu, Z.-H. Li, C.-Y. Chen, M. Baldo, and H.-J. Schulze, Convergence of the hole-line expansion with modern nucleon-nucleon potentials, Phys. Rev. C **96**, 044309 (2017).
[70] M. Kohno, Nuclear and neutron matter g-matrix calculations with a chiral effective field theory potential including effects of three-nucleon interactions, Phys. Rev. C **88**, 064005 (2013).
[71] D. Gerstung, Hyperons in nuclear matter and SU(3) chiral effective field theory, Ph.D. thesis, Technical University Munich (TUM), 2020.
[72] D. R. Entem and R. Machleidt, Accurate charge dependent nucleon nucleon potential at fourth order of chiral perturbation theory, Phys. Rev. C **68**, 041001(R) (2003).
[73] J. Hu (private communication).
[74] J. W. Holt, N. Kaiser, and W. Weise, Chiral three-nucleon interaction and the C-14 dating β decay, Phys. Rev. C **79**, 054331 (2009).
[75] J. W. Holt, N. Kaiser, and W. Weise, Density-dependent effective nucleon-nucleon interaction from chiral three-nucleon forces, Phys. Rev. C **81**, 024002 (2010).
[76] M. M. Nagels, T. A. Rijken, and Y. Yamamoto, Extended-soft-core baryon-baryon model ESC16. II. Hyperon-nucleon interactions, Phys. Rev. C **99**, 044003 (2019).
[77] A. Gal, E. V. Hungerford, and D. J. Millener, Strangeness in nuclear physics, Rev. Mod. Phys. **88**, 035004 (2016).
[78] E. Friedman and A. Gal, Λ Hypernuclear potentials beyond linear density dependence, Nucl. Phys. A **1039**, 122725 (2023).
[79] H. Krebs and E. Epelbaum, Toward consistent nuclear interactions from chiral lagrangians. II. Symmetry preserving regularization, Phys. Rev. C **110**, 044004 (2024).
[80] R. B. Wiringa, V. G. J. Stoks, and R. Schiavilla, An accurate nucleon-nucleon potential with charge independence breaking, Phys. Rev. C **51**, 38 (1995).
[81] F. Isaule, H. F. Arellano, and A. Rios, Di-neutrons in neutron matter within a Brueckner-Hartree-Fock approach, Phys. Rev. C **94**, 034004 (2016).
[82] A. Chorozidou and T. Gaitanos, Momentum dependence of in-medium potentials: A solution to the hyperon puzzle in neutron stars, Phys. Rev. C **109**, L032801 (2024).
[83] Y. Nara, A. Jinno, K. Murase, and A. Ohnishi, Directed flow of Λ in high-energy heavy-ion collisions and Λ potential in dense nuclear matter, Phys. Rev. C **106**, 044902 (2022).
[84] Y. Yamamoto, H. Bando, and J. Zofka, On the Λ hypernuclear single particle energies, Prog. Theor. Phys. **80**, 757 (1988).
[85] A. Jinno, K. Murase, Y. Nara, and A. Ohnishi, Repulsive Λ potentials in dense neutron star matter and binding energy of Λ in hypernuclei, Phys. Rev. C **108**, 065803 (2023).

[86] Y. Nogami and E. Satoh, Effect of Λ sigma conversion on the Λ-particle binding in nuclear matter, Nucl. Phys. B **19**, 93 (1970).
[87] A. R. Bodmer and D. M. Rote, Λ-N Σ-N coupling for Λ-N scattering and for the Λ-particle binding in nuclear matter, Nucl. Phys. A **169**, 1 (1971).
[88] J. Dabrowski, On the effect of ΛΣ conversion on the Λ particle binding energy in nuclear matter, Phys. Lett. B **47**, 306 (1973).
[89] Y. Fujiwara, Y. Suzuki, and C. Nakamoto, Baryon-baryon interactions in the SU(6) quark model and their applications to light nuclear systems, Prog. Part. Nucl. Phys. **58**, 439 (2007).
[90] I. Jaser Abualrob, *et al.*, Measurement of the p-Σ^+ correlation function in pp collisions at $\sqrt{s} = 13$ Tev, arXiv:2510.14448.
[91] A. Jinno, K. Murase, and Y. Nara, Λ and Σ potentials in neutron stars, hypernuclei, and heavy-ion collisions, arXiv:2501.09881.
[92] J. Mares, E. Friedman, A. Gal, and B. K. Jennings, Constraints on Σ nucleus dynamics from Dirac phenomenology of Σ-atoms, Nucl. Phys. A **594**, 311 (1995).
[93] J. Dabrowski, Isospin dependence of the single particle potential of the Σ hyperon in nuclear matter, Phys. Rev. C **60**, 025205 (1999).
[94] T. Harada and Y. Hirabayashi, Σ-production spectrum in the inclusive (π^-, K^+) reaction on ^{209}Bi and the Σ-nucleus potential, Nucl. Phys. A **767**, 206 (2006).
[95] M. Kohno, Y. Fujiwara, Y. Watanabe, K. Ogata, and M. Kawai, Semiclassical distorted wave model analysis of the (π^-, K^+) sigma formation inclusive spectrum, Phys. Rev. C **74**, 064613, 064613 (2006).
[96] T. Harada and Y. Hirabayashi, Production spectra with a Σ - hyperon in (π^-, K^+) reactions on light to heavy nuclei, Phys. Rev. C **107**, 054611 (2023).
[97] C. B. Dover, A. Gal, and D. J. Millener, Is isospin a good quantum number for Σ hypernuclei? Phys. Lett. B **138**, 337 (1984).
[98] M. Kohno and Y. Fujiwara, Localized N, Λ, Σ, and Ξ, Single-Particle potentials in finite nuclei calculated with SU(6) quark-model baryon-baryon interactions, Phys. Rev. C **79**, 054318 (2009).
[99] S. Binder, *et al.*, Few-nucleon systems with state-of-the-art chiral nucleon-nucleon forces, Phys. Rev. C **93**, 044002 (2016).
[100] H. Le, J. Haidenbauer, U.-G. Meißner, and A. Nogga, Separation energies of light Λ hypernuclei and their theoretical uncertainties, Eur. Phys. J. A **60**, 3 (2024).
[101] R. J. Furnstahl, N. Klco, D. R. Phillips, and S. Wesolowski, Quantifying truncation errors in effective field theory, Phys. Rev. C **92**, 024005 (2015).
[102] F. Sammarruca, L. Coraggio, J. W. Holt, N. Itaco, R. Machleidt, and L. E. Marcucci, Toward order-by-order calculations of the nuclear and neutron matter equations of state in chiral effective field theory, Phys. Rev. C **91**, 054311 (2015).
[103] X.-L. Shang, J.-M. Dong, W. Zuo, P. Yin, and U. Lombardo, Exact solution of the Brueckner-Bethe-Goldstone equation with three-body forces in nuclear matter, Phys. Rev. C **103**, 034316 (2021).
[104] J. A. Melendez, R. J. Furnstahl, D. R. Phillips, M. T. Pratola, and S. Wesolowski, Quantifying correlated truncation errors in effective field theory, Phys. Rev. C **100**, 044001 (2019).
[105] H. A. Bethe, Three-Body correlations in nuclear matter, Phys. Rev. **138**, B804 (1965).
[106] B. Day, Improved solution to the Bethe-Faddeev equations, Phys. Rev. **151**, 826 (1966).
[107] F. Sammarruca, L. E. Marcucci, L. Coraggio, J. W. Holt, N. Itaco, and R. Machleidt, Nuclear and neutron matter equations of state from high-quality potentials up to fifth order of the chiral expansion, arXiv:1807.06640.
[108] J. W. Holt, M. Kawaguchi, and N. Kaiser, Implementing chiral three-body forces in terms of medium-dependent two-body forces, Front. Phys. **8**, 100 (2020).
[109] S. Petschauer, J. Haidenbauer, N. Kaiser, U.-G. Meißner, and Wolfram Weise, Density-dependent effective baryonbaryon interaction from chiral three-baryon forces, Nucl. Phys. A **957**, 347 (2017).